Cell Death & Differentiation (2018) 25:1638–1656
https://doi.org/10.1038/s41418-018-0069-8

Cell Death & Differentiation

ARTICLE

SIRT2 regulates oxidative stress-induced cell death through deacetylation of c-Jun NH_2-terminal kinase

Mohsen Sarikhani[1] · Sneha Mishra[1] · Perumal Arumugam Desingu[1] · Chaithanya Kotyada[2] · Donald Wolfgeher[3] · Mahesh P. Gupta[4] · Mahavir Singh[2] · Nagalingam R. Sundaresan[1]

Received: 28 July 2017 / Revised: 6 December 2017 / Accepted: 15 January 2018 / Published online: 15 February 2018

Abstract

c-Jun NH_2-terminal kinases (JNKs) are responsive to stress stimuli and their activation regulate key cellular functions, including cell survival, growth, differentiation and aging. Previous studies demonstrate that activation of JNK requires dual phosphorylation by the mitogen-activated protein kinase kinases. However, other post-translational mechanisms involved in regulating the activity of JNK have been poorly understood. In this work, we studied the functional significance of reversible lysine acetylation in regulating the kinase activity of JNK. We found that the acetyl transferase p300 binds to, acetylates and inhibits kinase activity of JNK. Using tandem mass spectrometry, molecular modelling and molecular dynamics simulations, we found that acetylation of JNK at Lys153 would hinder the stable interactions of the negatively charged phosphates and prevent the adenosine binding to JNK. Our screening for the deacetylases found SIRT2 as a deacetylase for JNK. Mechanistically, SIRT2-dependent deacetylation enhances ATP binding and enzymatic activity of JNK towards c-Jun. Furthermore, SIRT2-mediated deacetylation favours the phosphorylation of JNK by MKK4, an upstream kinase. Our results indicate that deacetylation of JNK by SIRT2 promotes oxidative stress-induced cell death. Conversely, SIRT2 inhibition attenuates H_2O_2-mediated cell death in HeLa cells. SIRT2-deficient (SIRT2-KO) mice exhibit increased acetylation of JNK, which is associated with markedly reduced catalytic activity of JNK in the liver. Interestingly, SIRT2-KO mice were resistant to acetaminophen-induced liver toxicity. SIRT2-KO mice show lower cell death, minimal degenerative changes, improved liver function and survival following acetaminophen treatment. Overall, our work identifies SIRT2-mediated deacetylation of JNK as a critical regulator of cell survival during oxidative stress.

Introduction

c-Jun NH_2-terminal kinases (JNKs) were originally identified as stress-activated protein kinases that are encoded by three distinct genes. JNK1 and JNK2 are expressed in a variety of tissues, whereas JNK3 expression is restricted primarily to the brain, heart and testes [1, 2]. JNK is activated in response to a variety of stress stimuli, including DNA damage, growth factors, cytokines, oxidative and genotoxic stresses [3]. Previous studies found that activation of JNK requires dual phosphorylation by MKK4 and MKK7 on Thr183 and Tyr185 residues in a Thr-X-Tyr motif [2, 4]. The well-characterized targets of JNKs are mostly transcription factors and cell signalling proteins, including c-Jun, ATF2, IRS1 and Bcl-2 [1-4]. Though JNK activation requires phosphorylation, the other regulatory mechanisms behind JNK activation have been poorly understood. In cells, JNK activation results in a variety of outcomes, one of them being cell death [5]. The role of JNK

Edited by H Ichijo

Electronic supplementary material The online version of this article (https://doi.org/10.1038/s41418-018-0069-8) contains supplementary material, which is available to authorized users.

✉ Nagalingam R. Sundaresan
rsundaresan@iisc.ac.in

[1] Department of Microbiology and Cell Biology, Indian Institute of Science, Bengaluru, India

[2] Molecular Biophysics Unit, Indian Institute of Science, Bengaluru, India

[3] Department of Molecular Genetics and Cell Biology, University of Chicago, Chicago, IL, USA

[4] Department of Surgery, University of Chicago, Chicago, IL, USA

in promoting cell death was first established in neurons [6]. Similarly, JNK1$^{-/-}$/JNK2$^{-/-}$ mice were protected from ultraviolet (UV)-induced cell death [7]. Furthermore, virus-induced cell death occurs via JNK activation in HeLa cells [8]. JNK inhibitors have been shown to be protective against reactive oxygen species (ROS), mitochondrial dysfunction and cancer cell death [9]. Interestingly, JNK inhibitor reduced JNK activation and attenuated mitochondrial oxidant stress-induced cell death triggered by acetaminophen (APAP) toxicity, the most prevalent cause of drug-induced liver injury in western countries [10, 11].

Lysine acetylation is one of the reversible post-translational modifications linked to the pathogenesis of metabolic diseases [12]. Sirtuins are class III HDACs, which are homologues of the yeast Sir2 that requires NAD^+ as a cofactor. In mammals, seven sirtuin isoforms (SIRT1–7) having a common catalytic core domain but structurally different N- and C-terminal extensions have been characterized. Sirtuins protect against a variety of stress stimuli but mark the cells for death, in case of unrepairable damage. SIRT2 is predominantly localized in the cytoplasm. Like JNK, SIRT2 is also known to shuttle between cytoplasm and nucleus during stress [13]. SIRT2 regulates cell differentiation, growth, autophagy and cell cycle [14]. SIRT2-deficient (SIRT2-KO) mice have been shown to exhibit genomic instability and tumour in various organs [15]. Previous report suggests that oxidative stress increases SIRT2 levels in cells and induces cell death under severe stress conditions [16]. SIRT2 overexpression induces susceptibility to cell death and its inhibition induces tolerance against oxidative stress [17]. Similarly, Sirtuin 2 inhibition attenuates post-ischemic liver injury [18] and suppresses hepatic fibrosis induced by carbon tetrachloride and thioacetamide in mice [19].

In this work, we studied the role of reversible acetylation on regulating the activity of JNK. Our results indicate that the SIRT2 deacetylates Lys153 of JNK to enhance ATP binding, binding to upstream kinase and subsequently its catalytic activity. We found that SIRT2-mediated deacetylation of JNK regulates oxidative-stress-induced cell death in HeLa cells. Our results demonstrate that SIRT2-KO mice were protected against APAP-induced liver toxicity.

Results

Acetyltransferase p300 regulates lysine acetylation of JNK

To test whether JNK is an acetylated protein, we immunoprecipitated endogenous JNK and assessed acetylation status by western blotting (Fig. 1a). Similarly, we immunoprecipitated total cellular acetylated proteins with Ac-Lys antibody and probed for the JNK (Fig. 1b). Our results suggested that both JNK isoforms are acetylated proteins (Fig. 1a, b). Further, we found that treatment of Trichostatin A (TSA), a Class I and II histone deacetylase (HDAC) inhibitor, does not markedly influence the acetylation or phosphorylation of JNK, although we found mild increase in acetylation of JNK. However, treatment of nicotinamide (NAM), a class III HDAC inhibitor, markedly increased the acetylation levels of JNK and markedly reduced phosphorylation and activity of JNK, as assessed by the phosphorylation of c-Jun, a well-characterized target of JNK (Fig. 1c). Our short hairpin RNA (shRNA) screen results indicate that depletion of p300, but not other acetyl transferases, markedly increased the phosphorylation of JNK (Fig. 1d, e). Further results revealed that p300 strongly acetylates JNK, while p300/CBP-associated factor (PCAF) acetylates less efficiently in vitro (Fig. 1f). Hence, p300 was chosen for further experiments. Our findings indicate that p300 and JNK interacts with each other (Fig. 1g) and p300 depletion markedly reduced acetylation of JNK, while increasing the phosphorylation and catalytic activity of JNK towards c-Jun (Fig. 1h). Conversely, overexpression of p300 enhanced the acetylation of JNK, while reducing the phosphorylation and activity of JNK towards c-Jun in HeLa cells (Fig. 1i) and 293T cells (Figure S1a). Collectively, these results suggest that lysine acetylation of JNK by p300 reduces phosphorylation and catalytic activity of JNK.

SIRT2 deacetylase influences the enzymatic activity of JNK

In our initial experiments, treatment of NAM increased the acetylation, while reduced the JNK activity (Fig. 1c). Our screen for sirtuin isoforms found SIRT2 as JNK deacetylase, which can reduce the acetylation and enhance phosphorylation of JNK (Fig. 2a). Treatment of AGK2, an SIRT2 inhibitor, markedly increased acetylation, while reducing phosphorylation of JNK and activity towards c-Jun (Fig. 2b). Our further experiments suggested that SIRT2 interacts and co-localizes with JNK (Fig. 2c, d, Figure S1b). Interestingly, SIRT2 depletion enhanced acetylation, while reducing the phosphorylation and activity of JNK towards c-Jun (Fig. 2e). On the other hand, SIRT2 overexpression markedly reduced the acetylation of JNK but increased the phosphorylation of JNK (Fig. 2f, Figure S1c). Our in vitro kinase assay results show that SIRT2, but not SIRT2-H187Y, a catalytic inactive mutant, promotes catalytic activity of JNK towards c-Jun by deacetylation (Fig. 2g, h). Further luciferase reporter assay result suggested that SIRT2 depletion markedly reduces transcriptional activity of c-Jun (Figure S1d). Conversely, wild-type SIRT2, but not deacetylase-defective mutants of SIRT2 overexpression resulted in increased transcriptional activity of c-Jun

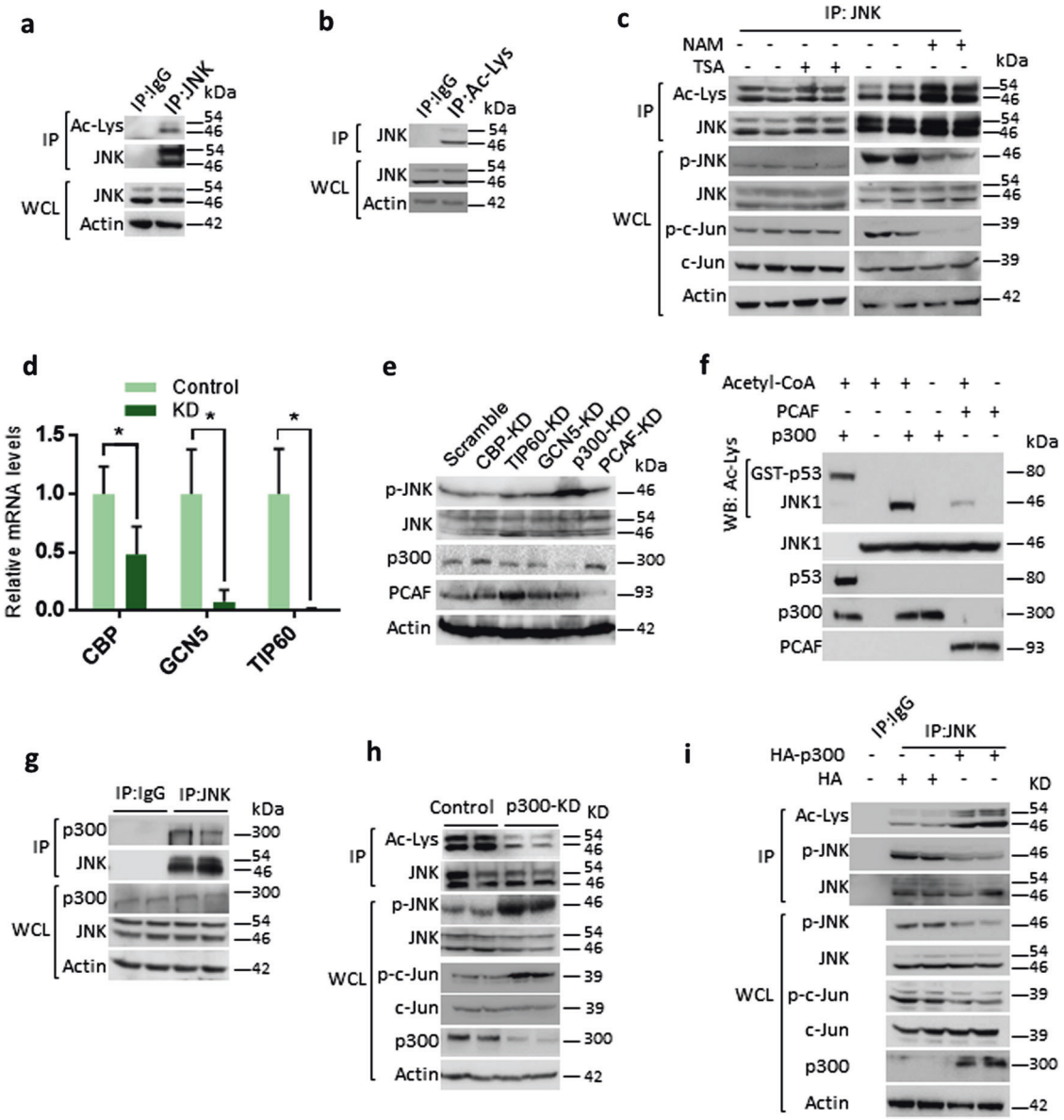

(Figure S1e). We found that SIRT2, but not catalytic inactive mutant, reduced the acetylation of JNK (Figure S1f). These results indicate that SIRT2 regulates endogenous activity of JNK by regulating its phosphorylation. To translate these in vitro findings in vivo, we analysed the levels of JNK acetylation and its phosphorylation in wild-type and SIRT2-KO mice. We found increased acetylation and decreased phosphorylation of JNK in the liver of SIRT2-KO mice (Fig. 2i, j). Similarly, SIRT2-KO mice liver tissue samples exhibited reduced phosphorylation of c-Jun, indicating reduced activity of JNK in SIRT2-KO conditions (Fig. 2j). Interestingly, the mRNA levels of c-Jun target genes, p53 and p16, were significantly low in the SIRT2-KO liver, suggesting that SIRT2 deficiency reduced c-Jun activity, which might be linked to the impaired activity of JNK.

Deacetylation of JNK favours phosphorylation by upstream kinase, MKK4

Previous studies have shown that JNK shuttles between nucleus and cytoplasm [20]. Our confocal microscopic analysis suggested inhibition of SIRT2 by AGK2 do not influence the localization of green fluorescent protein (GFP)-JNK1 (Figure S1g). On the similar lines, overexpression of neither wild-type SIRT2 nor deacetylase activity-defective mutants of SIRT2 changes localization of GFP-JNK1 (Figure S1h). These results suggested that acetylation has no effect on JNK sub-cellular localisation. Earlier works have demonstrated that SIRT2 regulates cellular functions by transcriptional regulation [21]. However, our results suggested that SIRT2-KO mice does not show any changes in the expression levels of JNK isoforms in the

◀ **Fig. 1** p300 acetyltransferase play key role in regulating JNK acetylation and activity. **a** Western blotting analysis showing the acetylation of endogenous JNK in HEK 293T cells. Endogenous JNK was immunoprecipitated and acetylation was detected by western blotting using pan-acetyl lysine antibody. Whole-cell lysates (WCLs) of 293T cells were probed for JNK and actin. $n = 3$ independent experiments. **b** Western blotting analysis depicting the acetylation status of JNK in 293T cells. Endogenous acetylated proteins were immunoprecipitated with anti-pan acetyl lysine antibody and probed for JNK by western blotting. WCLs of 293T cells were probed for JNK and actin. $n = 3$ independent experiments. **c** Western blot analysis showing the acetylation, phosphorylation status and activity of JNK in cells treated with Class I and II HDAC inhibitor, Trichostatin A (TSA) or Class III HDAC inhibitor, nicotinamide (NAM). 293T cells were treated with vehicle or 10 μM TSA for 12 h. 293T cells were treated with vehicle or 50 mM NAM for 6 h. Acetylation was assessed by immunoprecipitating endogenous JNK with a specific JNK antibody. The WCL was tested for the phosphorylation of JNK by western blotting. The activity of endogenous JNK was tested by measuring the phosphorylation of c-Jun, a downstream transcription factor of JNK. $n = 4$ independent experiments. **d** Graph showing the relative mRNA expression levels of acetyl transferases, CBP, GCN5 and TIP60 in HeLa cells treated with either scramble (control) or specific pool of shRNAs targeting individual acetyl transferases, as measured by real-time qPCR analysis. $n = 3$–4 samples per group. Data are presented as mean ± s.d. $^*p < 0.05$. Student's *t*-test was used to calculate the *p*-values. **e** Western blotting analysis showing the phosphorylation status and activity of JNK in HeLa cells treated with scramble or specific pool of shRNAs targeting individual acetyl transferases. The WCL was used to check the phosphorylation of JNK by western blotting. Depletion of p300 or PCAF was tested by assessing their protein levels by western blotting with specific antibodies. The depletion of acetyl transferases, CBP, GCN5 and Tip60 was assessed by measuring the mRNA levels, as shown in Fig. 1d, due to lack of specific antibodies. **f** Western blotting analysis showing in vitro acetylation of JNK by p300. Purified recombinant JNK was used as a substrate for acetyltransferases p300 and PCAF in the presence or absence of acetyl CoA. The acetylation of JNK was assessed by western blotting with pan-acetyl lysine antibody. Recombinant p53 was used as a positive control for acetylation assay. Recombinant p300 strongly acetylates JNK, when compared to PCAF, as assessed by western blotting. **g** Endogenous JNK was immunoprecipitated and probed for its interaction with p300 by western blotting. IgG was used as negative control. WCLs were probed for the presence of JNK and p300 by western blotting. **h** Western blotting analysis showing acetylation, phosphorylation and activity of JNK in HeLa cells expressing luciferase shRNA (control) or p300 shRNA (p300-KD). WCLs were probed for the depletion of p300 by western blotting. JNK was immunoprecipitated and probed for Ac-Lys antibody. JNK activity was measured by assessing the phosphorylation of c-Jun. Specific antibody was used to detect the phosphorylation of JNK. **i** Western blotting analysis showing acetylation and phosphorylation of JNK in HeLa cells overexpressing HA-p300. JNK was immunoprecipitated from HeLa cells transiently overexpressing p300 were analysed for the acetylation and phosphorylation levels of JNK by western blotting. WCLs were probed for the overexpression of p300

liver (Fig. 3a). Similarly, overexpression of SIRT2 does not modulate the mRNA levels of JNK isoforms (Figure S1i). In addition, SIRT2 deficiency does not change the expression of upstream kinases and phosphates, previously known to regulate the activity of JNK in liver samples (Fig. 3b). Similarly, SIRT2 overexpression does not change the protein levels of upstream phosphates and phosphorylation of MKK4 (Fig. 3c). Collectively these findings suggested that SIRT2 deficiency or overexpression do not alter the expression of JNK or its upstream kinases and phosphates. Most likely, SIRT2 might exclusively regulate JNK through reversible acetylation. Under stress conditions, activation of JNK is mediated by upstream kinases MKK4 [4]. We do not observe any significant changes in the interaction between MKK4 and JNK in the SIRT2-overexpressed cells (Fig. 3d), suggesting that SIRT2 do not influence the binding of MKK4 with JNK. Next, we tested whether deacetylation of JNK affect the ability of MKK4 to phosphorylate JNK and found that deacetylation favours the phosphorylation of JNK by MKK4 (Fig. 3e). To verify these findings, we tested the MKK4-dependent phosphorylation of JNK in cells overexpressed with SIRT2 or its catalytic mutant, SIRT2-H187Y. Consistent with previous results, we found that SIRT2 overexpression enhances the MKK4-dependent phosphorylation of JNK in a deacetylase activity-dependent manner (Fig. 3f). These findings suggest that SIRT2 favours the phosphorylation of JNK by its upstream kinase MKK4.

Tandem mass spectrometry, molecular modelling and molecular dynamics simulations indicate that acetylation of JNK at Lys153 regulate ATP binding

Proteomic analysis identified six different acetylated lysine residues in JNK1 (Lys30, 153, 160, 166, 265 and 308) (Figure S2a). Further homology alignment indicated that Lys153 and Lys166 are conserved across diverse species (Figure S2b) and across JNK isoforms (Figure S2c), suggesting a possibility that all isoforms of JNK may be regulated by reversible acetylation. Indeed, our western blotting analysis indicate the acetylation of all JNK isoforms (Fig. 1c, h, j). Further, stoichiometric analysis of acetylation for Lys153 and Lys166 was 3.37% and 4.63%, respectively (Figure S2d). To delineate the structural basis for the effect of acetylation on the binding of adenine nucleotide to the pocket of JNK, we modelled in silico acetylation on the side chain of K151 of wild-type crystal structure (PDB ID 4QTD). The modelled structure suggests that the acetylated side chain of K151 in JNK will be in close proximity to the negatively charged phosphates of the modelled adenosine triphosphate (ATP) nucleotide and magnesium ion to have stearic affects (Fig. 4a). Therefore, we assumed that the proximal location of the bulky acetylated side chain of K151 might hamper the binding of the adenosine nucleotide to the pocket of JNK.

Further, to comprehend the effect of acetylation on the binding of adenosine nucleotide to the pocket of JNK, we performed MD simulations of the wild-type and acK151 mutant of JNK, respectively. The production run of two independent trajectories of each system indicate a stable

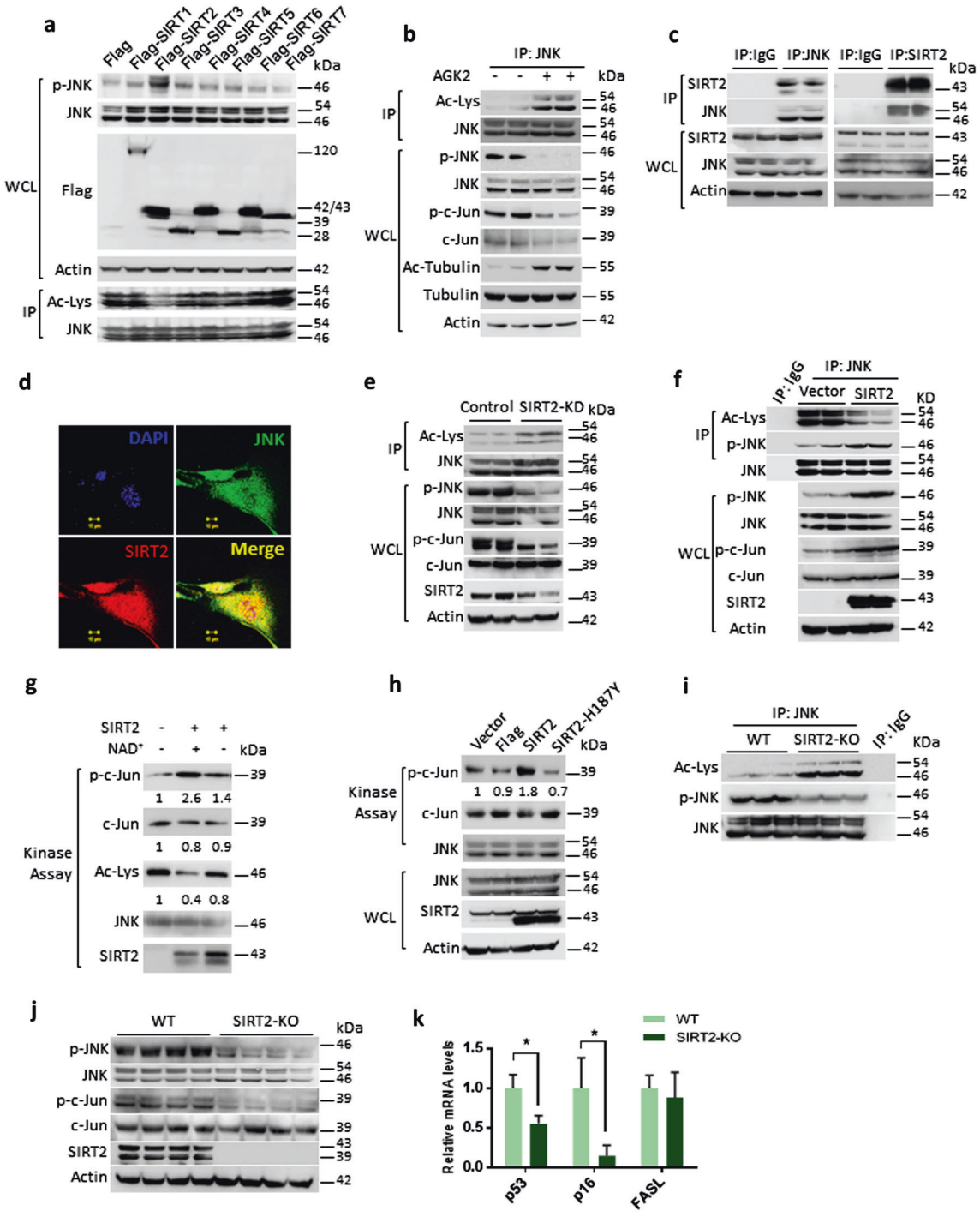

root mean square deviation (RMSD) of backbone Cα atoms ranging between 0.1 and 0.3 nm (Fig. 4b). Further, we observed similar root means square fluctuation (RMSF) values in the two trajectories for the backbone Cα atoms of each system (Figure S3a, S3b). However, visual analysis of the trajectories showed significant displacement of the ATP nucleotide in the acetylated mutant while in contrast the γ-phosphate of the ATP nucleotide in the wild-type moved closer to the side chain of K151 residue (Fig. 4c). In agreement, the RMSD value for the adenosine nucleotide is moderately higher in both the trajectories of the acetylated mutant compared to the wild type (Fig. 4d). For analysis, we used one of the stable trajectory of the wild type (dark green) and acK153 (dark blue), respectively. To quantify the nucleotide displacement effect, we plotted the distance between the nitrogen atom of side chain amine in K153 and acK153 with the γ-phosphate of ATP nucleotide (Fig. 4e). Figure 4e illustrates a considerable variation in the distances

◀ **Fig. 2** SIRT2 deacetylase regulates the acetylation of JNK. **a** Western blotting analysis showing acetylation and phosphorylation of JNK in HeLa cells overexpressing the Sirtuin isoforms, SIRT1–SIRT7. Cells were transiently overexpressed with either Flag- or Flag- SIRT1-7, and phosphorylation of JNK was analysed by western blotting. JNK was immunoprecipitated from these overexpressed lysates and tested for its acetylation by western blotting. Whole-cell lysates (WCLs) were probed with Flag-antibody for detecting the expression of Sirtuins. **b** Western blotting analysis showing the phosphorylation, acetylation and activity of JNK in HeLa cells treated with vehicle or SIRT2 inhibitor, 10 μM AGK2 for 6 h. The activity of AGK2 was tested by probing the acetylation status of tubulin with specific antibody detecting the acetyl-tubulin. JNK was immunoprecipitated from the WCLs and probed for Ac-Lys antibody. The phosphorylation of JNK was tested by western blotting. The activity of JNK was tested by detecting the phosphorylation of c-Jun with specific antibody. **c** Endogenous JNK or SIRT2 was immunoprecipitated and probed for its interaction with SIRT2 or JNK respectively, by western blotting. IgG was used as negative control. WCLs were probed for the presence of JNK and SIRT2 by western blotting. Actin was used as a loading control. **d** Co-localization of JNK (green) with SIRT2 (red), as determined by confocal microscopy. Endogenous JNK and SIRT2 were stained using specific antibodies. The merged image shows yellow colour, indicating the co-localization of JNK and SIRT2, both in the cytoplasm and the nucleus. Scale bar = 10 μM. **e** Western blotting analysis showing acetylation, phosphorylation and activity of JNK in cells expressing scramble shRNA (control) or SIRT2 shRNA (SIRT2-KD). WCLs were probed for the depletion of SIRT2 by western blotting. JNK was immunoprecipitated and probed with Ac-Lys antibody to detect the acetylation. JNK activity was measured by detecting the phosphorylation of c-Jun by western blotting. Phosphorylation of JNK was detected with the use of a specific antibody. **f** Western blotting images depicting acetylation, phosphorylation and activity of JNK in HeLa cells overexpressing either control vector or SIRT2. WCLs were probed for the overexpression of SIRT2 by western blotting. JNK was immunoprecipitated and probed with Ac-Lys antibody to detect the acetylation. JNK activity was measured by detecting the phosphorylation of c-Jun by western blotting. The phosphorylation of JNK was detected by a specific antibody. **g** Representative western blotting images showing in vitro kinase assay for recombinant acetylated and deacetylated JNK1. Endogenously acetylated JNK1 was incubated with SIRT2 in the presence and absence of NAD^+ in a test tube for deacetylation. Then the enzymatic activity of acetylated and deacetylated JNK1 against the c-Jun-fusion protein, which contains the JNK-specific phosphorylation site. $n = 3$ independent experiments. **h** Representative western blotting images depicting in vitro kinase assay for endogenous JNK immunoprecipitated from HeLa cells overexpressing either control vector, Flag, SIRT2 or SIRT2-H187Y. Immunoprecipitated JNK was incubated with c-Jun fusion protein to assess the enzymatic activity and the phosphorylation of c-Jun was analysed by western blotting. WCLs were probed for the overexpression of SIRT2 and endogenous JNK levels by western blotting. **i** Representative western blotting analysis showing acetylation and phosphorylation of JNK immunoprecipitated from wild-type (WT) and SIRT2-deficient (SIRT2-KO) mice. Liver tissue lysate of WT and SIRT2-KO mice was analysed for acetylation and phosphorylation of JNK by western blotting. $n = 5$ mice per group. **j** Representative western blotting images showing phosphorylation and activity of JNK in liver lysates of WT and SIRT2-KO mice. Tissue lysates of WT and SIRT2-KO mice was analysed for phosphorylation of JNK and SIRT2 levels. JNK activity was measured by detecting the phosphorylation of c-Jun. Actin was used as a loading control. $n = 8$ mice per group. **k** Graph depicting the relative mRNA expression levels of AP-1 target genes, p53, p16 and FasL in WT and SIRT2-KO mice, as measured by real-time qPCR analysis. $n = 3$–4 mice per group. Data are presented as mean ± s.d. $^*p < 0.05$. Student's *t*-test was used to calculate the *p*-values

between these two atoms in the acetylated mutant compared to the wild type. As previously visualized in the wild type, the negatively charged phosphate of the ATP nucleotide moves closer to the nitrogen atom in the amine side chain of K153 residue within 10 ns (Fig. 4c, e). The significantly higher distance between the side chain nitrogen atom of acK153 and γ-phosphate of adenosine tri-phosphate clearly indicates that the neutralization of positive charge in the side chain amine, coupled with the stearic occlusion caused by the bulky acetylated side chain, affects the binding of the nucleotide to the pocket of the acK153 mutant.

K153 is absolutely conserved and mostly buried residue in JNK (Fig. 4a). Surprisingly, our experimental results showed improved binding of the ATP in the K151R mutant of JNK. To gain structural insight into the K153R mutant, we generated an in silico structural model of K153R that was further energy minimized. The energy-minimized structure of R153 shows that the arginine side chain adopts a conformation very similar to K153 in wild-type JNK. The arginine side chain is well fitted in place of lysine in the structure. Also, the orientation and distance between the side chain NH2 of R153 and O3G atom of γ-phosphate is similar to the side chain NZ of K153 and O3G atom of γ-phosphate (Fig. 4f). Therefore, we argue that it is plausible that JNK K153R mutant will have ATP binding and activity similar to the wild type JNK (Fig. 4f).

To test whether acetylation regulate the ATP binding to JNK, we performed ATP-binding assays with either [α^{32}-P] or [γ^{32}-P] ATP. Total counts per minute and dot blot analysis obtained in a scintillation counter indicated JNK1-K153R mutant binds to ATP at higher levels than wild-type or K153Q mutants of JNK1 (Fig. 4g, Figure S3c). These findings suggested that acetylation of Lys153 impairs binding to ATP. Our further results suggest that SIRT2 overexpression do not markedly change the activity of JNK-K153R or K153Q mutants (Figure S3d), indicating that K153 may be the deacetylation target of SIRT2. We found that mutation of Lys153 to Arg153 (JNK1-K153R) increased the phosphorylation and activity of JNK (Fig. 4h). However, we do not see any change in the phosphorylation and acetylation of JNK, when wild-type JNK mutated to either K166R or K166Q (Figure S3e). Moreover, our luciferase assay results suggested JNK1-K153R is fourfold more active than JNK-K153Q towards c-Jun (Fig. 4i). These results indicate that Lys153 acetylation of JNK inhibits ATP binding and thus impairs the catalytic activity of JNK.

SIRT2 dynamically regulates JNK acetylation during cellular stress

We treated cells with H_2O_2 (oxidative stress) or exposed to UV (genotoxic stress) to study the effect of acetylation on

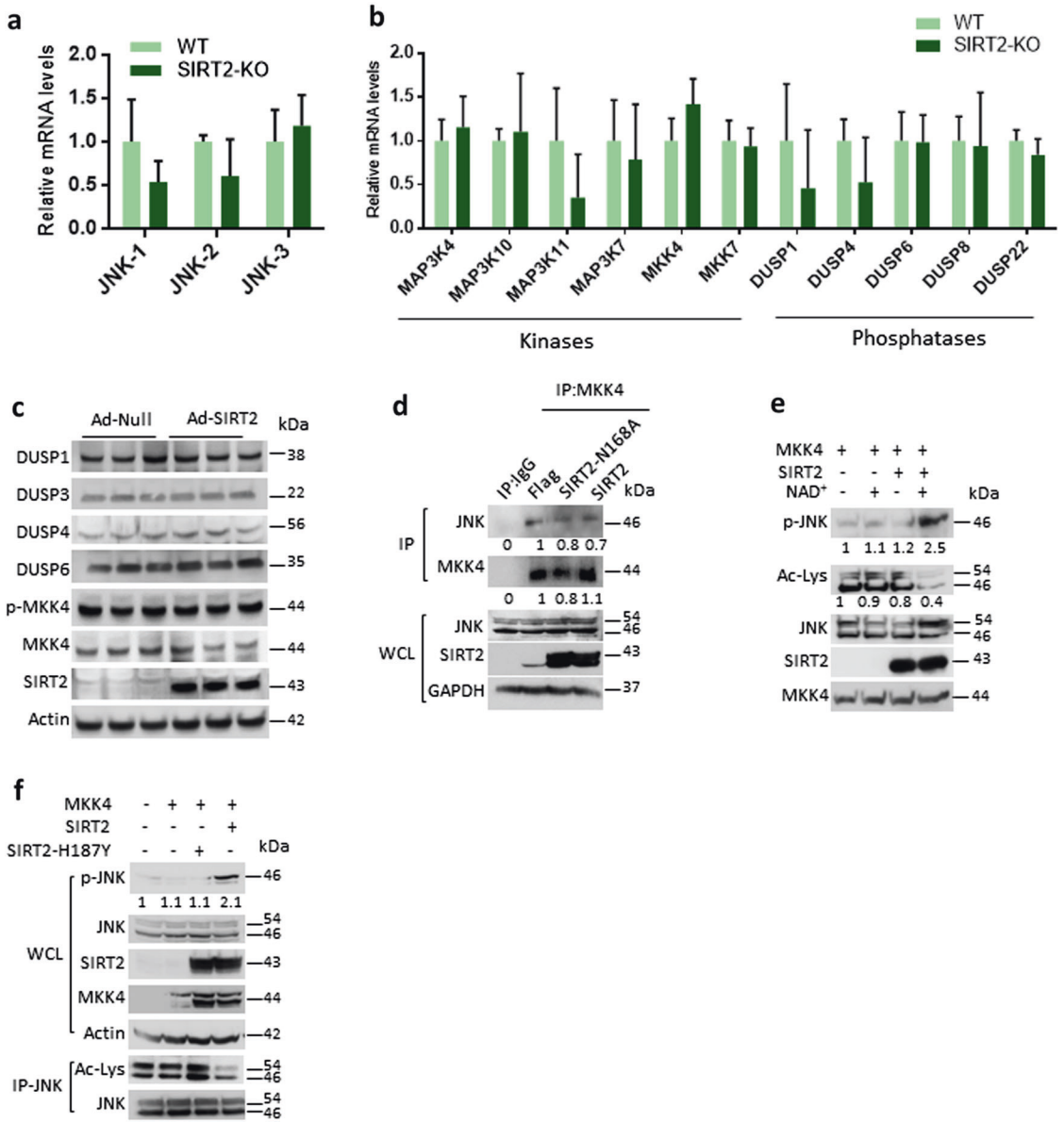

Fig. 3 Deacetylation favours MKK4-dependent activation of JNK. **a** Graph showing the relative mRNA expression levels of JNK isoforms in wild-type (WT) and SIRT2-deficient (SIRT2-KO) mice, as measured by real-time qPCR analysis. $n = 3$–4 mice per group. Data are presented as mean ± s.d. $^*p < 0.05$. Student's *t*-test was used to calculate the *p*-values. **b** Graph showing the relative mRNA expression levels of JNK upstream kinases and phosphates in WT and SIRT2-KO mice, as measured by real-time qPCR analysis. $n = 3$–4 mice per group. Data are presented as mean ± s.d. $^*p < 0.05$. Student's *t*-test was used to calculate the *p*-values. **c** Western blotting images showing the expression of JNK upstream phosphates in HeLa cells overexpressing either control (Ad-Null) or SIRT2 (Ad-SIRT2). Similarly, the phosphorylation of MKK4, an upstream kinase of JNK, was measured by western blotting. $n = 3$ independent experiments. **d** Representative western blotting images showing MKK4 interaction with JNK. MKK4 was immunoprecipitated from cells transiently expressing SIRT2 or SIRT2-N168A mutant and probed for JNK by western blotting. Whole-cell lysates (WCLs) were probed for the overexpression of SIRT2 and endogenous JNK levels by western blotting. $n = 3$ independent experiments. **e** Representative western blotting images showing the effect of acetylation on the MKK4-mediated phosphorylation of JNK. Endogenous acetylated JNK was immunoprecipitated from HeLa cells treated with deacetylase inhibitors. The acetyl-JNK was further incubated with SIRT2 in the presence or absence of NAD^+ in a test tube and then subjected to a kinase assay, where deacetylated JNK was used as substrate for MKK4. Phosphorylation and acetylation of JNK were assessed using western blotting. $n = 3$ independent experiments. **f** Representative western blotting images showing the effect of SIRT2-mediated deacetylation on the MKK4-dependent phosphorylation of JNK. MKK4 was overexpressed in HeLa cells transiently expressing either SIRT2 or SIRT2-H187Y. WCLs were probed for the overexpression of SIRT2, SIRT2-H187Y and MKK4. Endogenous JNK levels and its phosphorylation was assessed by western blotting. Lower panel shows the acetylation status of JNK assessed by western blotting

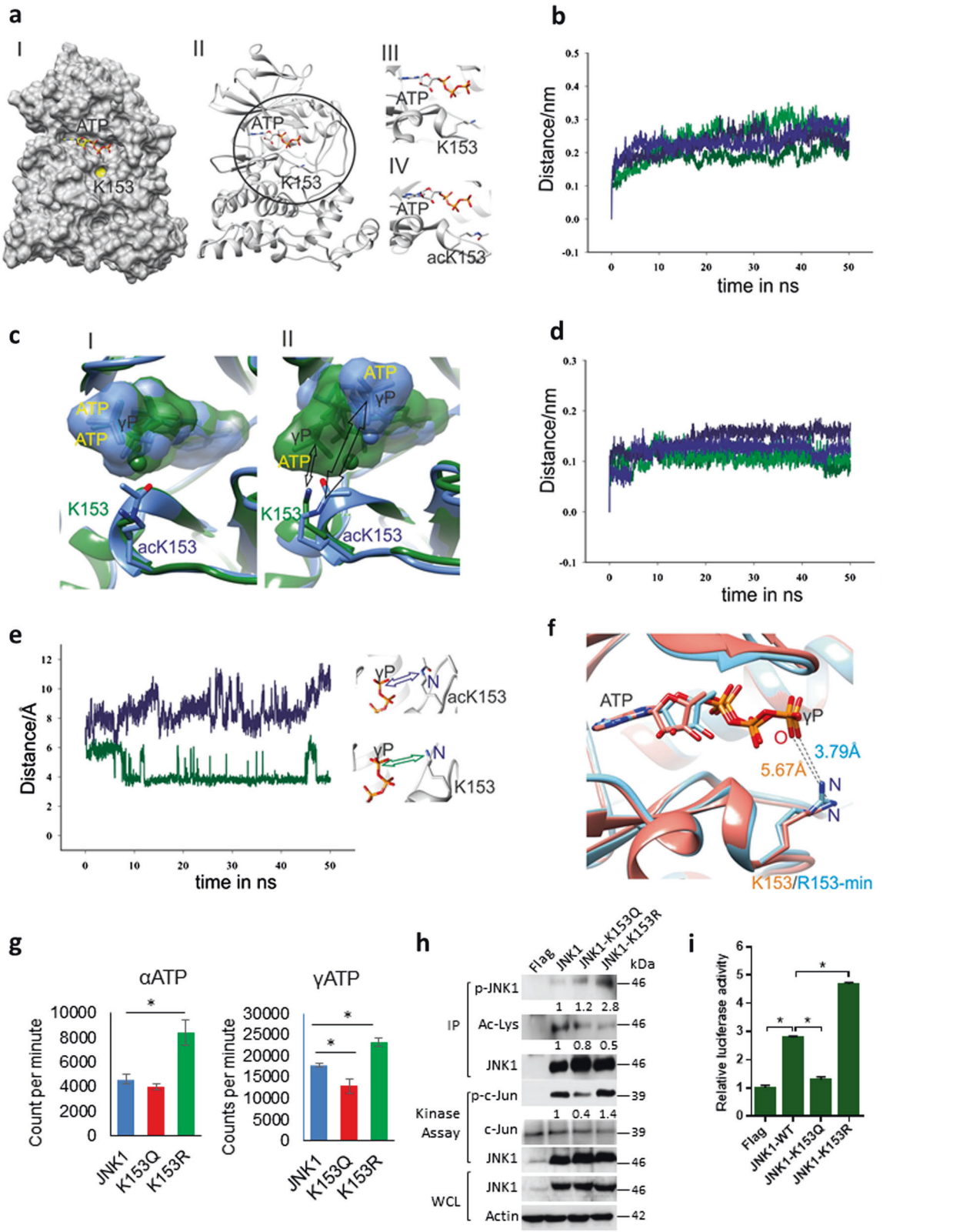

stress-dependent activity of JNK. Treatment with H_2O_2 at two different concentrations, increased the phosphorylation of JNK and its catalytic activity towards c-Jun (Fig. 5a, b, Figure S3f). Similar results were observed after UV exposure, another known activator of JNK [7, 22] (Fig. 5c). Interestingly, H_2O_2 treatment elevated SIRT2 levels, while

◀ **Fig. 4** Modelling and molecular dynamic simulations of JNK. **a** Representation of the acetylation site on the crystal structure of JNK (PDB ID 4QTD) (I) surface, (II) cartoon and (III) magnified active site representing position of K153 (IV) magnified active site representing position of acetylated K153 (acK153). **b** Overlay of protein backbone Cα RMSD plots of the wild-type (dark green, light green) and acK153 mutant (dark blue, light blue) of JNK. **c** Overlay of the wild-type (green) and acK153 mutant (blue) of JNK representing the surface of ATP nucleotide at the (I) start of production run and (II) random snapshot after 10 ns in the MD trajectory. **d** Overlay of ATP nucleotide RMSD plots of the wild-type (dark green, light green) and acK153 mutant (dark blue, light blue) of JNK. **e** Overlay of the distance between and γ-phosphate of ATP and nitrogen atom side-chain amine in K153 (dark green) and acK153 (dark blue) as a function of time for the two systems. **f** Overlay of the structures of JNK wild-type (salmon, K153) and energy-minimized structures of K153R mutant (blue, R153-min). The distance between the oxygen (O3G) atom of γ-phosphate of ATP and side-chain nitrogen atom (NZ) of K153 in wild-type JNK and side-chain NH2 atom of energy-minimized R153 are shown. **g** Graph showing binding of ATP to recombinant GST-tagged wild-type and mutants of JNK1, JNK1-K153Q and JNK1-K153R. GST-tagged proteins were purified from *E. coli* BL21 (DE3) and was incubated with either [α-^{32}P] or [γ-^{32}P] ATP. The unbound ATP was washed, and the bound ATP was measured in a scintillation counter and reported as counts per minute (cpm). $n = 6$ independent experiments. Data are presented as mean ± s.d. $^*p < 0.05$. One-way ANOVA was used to calculate the *p*-values. **h** Representative western blotting images depicting in vitro kinase assay for wild-type JNK1, JNK1-K153Q and JNK1-K153R. The wild-type and mutants of JNK1 were immunoprecipitated using Flag-antibody-conjugated agarose beads and incubated with c-Jun fusion protein in an in vitro kinase assay. JNK activity was measured by detecting the phosphorylation of c-Jun. The acetylation and phosphorylation of immunoprecipitated JNK was probed by western blotting. Whole-cell lysates (WCLs) were probed for JNK by western blotting. **i** Graph showing luciferase reporter assay to analyse JNK activity in HeLa cell transiently expressing either JNK1 or JNK1-K153Q or JNK1-K153R. Reporter plasmid containing multiple binding sites for AP-1 was used to track the activity of JNK in HeLa cells. $n = 3$ independent experiments. Data are presented as mean ± s.d. $^*p < 0.05$. One-way ANOVA was used to calculate the *p*-values

acetylation of tubulin-K40 was reduced (Fig. 5a). We observed time-dependent increase in the phosphorylation, which corresponds to reduced acetylation of JNK following H_2O_2 treatment (Fig. 5b). Similar deacetylation of JNK was observed in cells exposed to UV (Fig. 5c). Our results suggest that p300 overexpression inhibits JNK phosphorylation and catalytic activity under both basal and stress conditions (Fig. 5d). In addition, SIRT2 overexpression increased the phosphorylation and activity of JNK during cellular stress (Figure S3g), suggesting that SIRT2 augments JNK activity during stress. Interestingly, we found increased levels of SIRT2 in stress conditions (Fig. 5a–c), suggesting that SIRT2 might be stabilized in oxidative and genotoxic stress. Collectively, these results suggest that acetylation of JNK is dynamically regulated by SIRT2 and p300 during oxidative and genotoxic stress. We found that SIRT2 deficiency or SIRT2 inhibition by AGK2 impairs the H_2O_2-induced phosphorylation of JNK, which is associated with failure of deacetylation of JNK (Fig. 5e, f). Interestingly, JNK-K153R mutant show enhanced, whereas JNK-K153Q mutant exhibit reduced H_2O_2-induced phosphorylation (Fig. 5g). Overall, these results suggest that SIRT2 is required for H_2O_2-mediated deacetylation and activation of JNK.

JNK deacetylation by SIRT2 promotes stress-induced cell death

Previous studies suggested that JNK plays a critical role in cell survival [22, 23]. Inhibition of JNK has been shown to protect HeLa cells against H_2O_2-induced cell death [24, 25]. Our results suggested that SIRT2-depleted cells were significantly resistant to H_2O_2-induced cell death (Fig. 6a–c) and show reduced transcriptional activity of c-Jun following H_2O_2 treatment (Fig. 6d). Conversely, overexpression of wild type but not catalytic inactive mutants of SIRT2 increased the susceptibility of HeLa cells to H_2O_2-induced cell death (Fig. 6e–g). Like our previous findings, both inhibition or depletion of SIRT2 enhanced the cell survival following H_2O_2 treatment (Figure S4a, S4b). On the other hand, SIRT2 overexpression resulted in 43% reduction in cell survival after H_2O_2 treatment (Figure S4c). These findings indicate that SIRT2 is required for the H_2O_2-induced cell death in HeLa cells. Further results indicate that overexpression of JNK1-K153R resulted in reduction in cell survival, whereas JNK1-K153Q promoted cell survival following H_2O_2 treatment (Figure S4d, S4e and S4f). Consistently, we have observed enhanced c-Jun transcriptional activity in cells overexpressing JNK-K153R (Figure S4g). Next, we tested whether JNK-mediated cell death is linked to SIRT2-mediated deacetylation of JNK. Interestingly, treatment of SP600125, a JNK-specific inhibitor, markedly reduces the JNK activity and partially rescued the SIRT2-mediated increase in H_2O_2-induced cell death and promoted survival (Fig. 6h–k, Figure S4h), suggesting that SIRT2-mediated deacetylation of JNK might be partly involved in H_2O_2-induced cell death.

SIRT2-KO mice were resistant to hepatotoxicity induced by APAP

APAP overdose causes severe hepatotoxicity in animals and humans. Although the pathophysiology of APAP-induced hepatotoxicity is complex, studies indicate that oxidative stress-induced activation of JNK acts downstream of APAP metabolism to promote cell death, degenerative changes and impaired function of the liver [11, 26, 27]. Therefore, we tested the susceptibility of SIRT2-KO mice to low dose of APAP (200 mg/kg). Histology analysis indicated that SIRT2-KO mice were resistant to liver injury and degenerative changes (Fig. 7a). Moreover, SIRT2-KO mice were

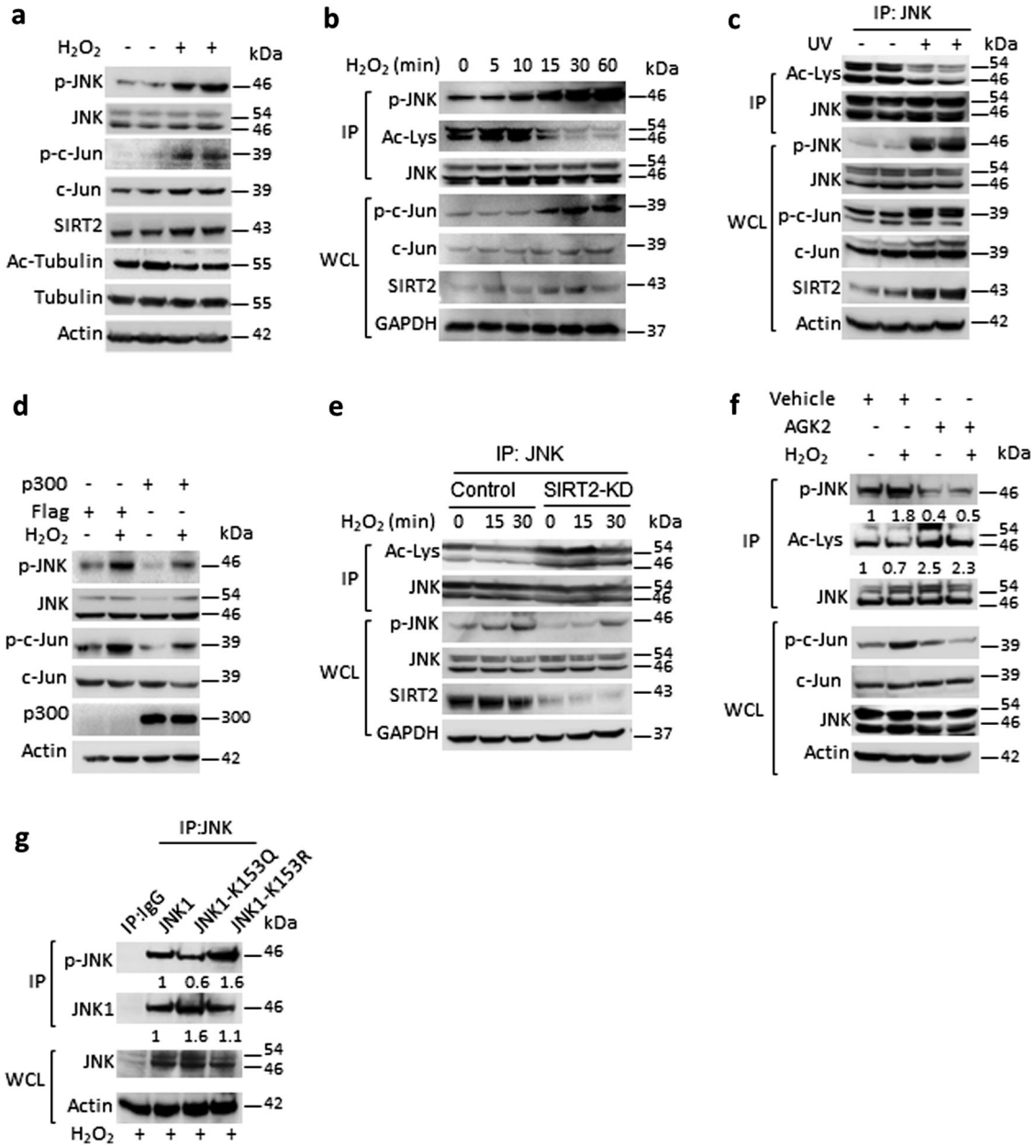

resistant to cell death induced by APAP (Fig. 7b, c). Assessment of liver function supported the histological findings of less susceptibility of SIRT2-KO mice to APAP hepatotoxicity (Fig. 7d, e). Western blotting analysis of JNK acetylation and phosphorylation in the liver lysates of wild-type mice indicated that APAP treatment reduced the acetylation and thus increased the phosphorylation of JNK (Fig. 7f, g). However, SIRT2 deficiency impaired the activation of JNK due to elevated acetylation found in the liver lysates (Fig. 7f, g). Next, to assess the overall survival rate of mice following the acute toxicity, we used a high dose of APAP (600 mg/kg). Treatment of mice with high doses of APAP resulted in 100% death within 6 h in wild-type mice. However, SIRT2-KO mice were resistant and only 30% died at 6 h; 15% were alive even up to 48 h post treatment of 600 mg/kg APAP. These findings collectively indicate that SIRT2 deficiency might protect the liver by reduced activation of JNK following APAP toxicity.

Discussion

Our work establishes reversible acetylation as a novel post-translational mechanism that regulates the kinase activity of JNK. Our findings suggest that SIRT2-mediated deacetylation is essential for basal and stress-induced activation of

◀ **Fig. 5** Reversible acetylation of K153 regulates ATP binding and kinase activity of JNK. **a** Western blotting images showing the phosphorylation of JNK, c-Jun and total protein levels of SIRT2 and K-40 tubulin acetylation in HeLa cells treated with 200 μM H_2O_2 for 30 min. $n = 4$ independent experiments. **b** Western blotting images showing the time-dependent phosphorylation, acetylation and activity of JNK upon H_2O_2 treatment. HeLa cells were treated with 500 μM H_2O_2 for different time points and the JNK immunoprecipitated from these cells were analysed for their acetylation and phosphorylation levels by western blotting. The whole-cell lysate (WCL) was used to observe the concomitant changes in the phosphorylation of c-Jun, a downstream target of JNK. **c** Western blotting images showing the UV-induced changes in phosphorylation, acetylation and activity of JNK. JNK was immunoprecipitated from HeLa cells treated with UV (1 KJ/m^2) for 30 min and assessed for acetylation. WCLs were probed for phosphorylation of JNK, phosphorylation of c-Jun and total protein levels of SIRT2 by western blotting. $n = 3$ independent experiments. **d** Western blotting images depicting the effect of p300 overexpression on H_2O_2-mediated phosphorylation and activity of JNK. 293T cells transiently overexpressing p300 were treated with 500 μM H_2O_2 for 30 min, and the phosphorylation of JNK and c-Jun were analysed by western blotting. **e** Western blotting images showing the effect of SIRT2 depletion on H_2O_2-mediated phosphorylation and acetylation of JNK. SIRT2-depleted HeLa cells were treated with 500 μM H_2O_2 for 30 min for different time points. JNK was immunoprecipitated and assessed for the acetylation of JNK. WCLs were probed for phosphorylation of JNK and total protein levels of SIRT2 by western blotting. **f** Western blotting images depicting the effect of SIRT2 inhibition on H_2O_2-mediated phosphorylation, acetylation and activity of JNK. HeLa cells were treated with 10 μM AGK2 for 2 h and then treated with 500 μM H_2O_2 for 30 min. The phosphorylation of c-Jun was analysed by western blotting in WCLs. JNK was immunoprecipitated from HeLa cells and assessed for acetylation and phosphorylation. **g** Representative western blotting images showing H_2O_2-mediated phosphorylation of wild-type and mutants of JNK. HeLa cells transiently expressing JNK1 or JNK1-K153Q or JNK1-K153R were treated with 500 μM H_2O_2 for 30 min. JNK was immunoprecipitated from these lysates and assessed for its phosphorylation by western blotting

JNK. We propose that SIRT2-mediated deacetylation of JNK promotes ATP binding and upstream kinase activity on JNK. The proposed mechanism supports the role of JNK in oxidative stress-induced HeLa cell death and APAP-induced hepatotoxicity.

Several upstream signals are known to activate JNK. It is possible that JNK will not be able to respond to upstream signals, if it is constitutively acetylated. We believe that acetylation may be the first line of control for JNK activity, as found in other non-histone proteins like p53 and AKT [28, 29]. It is worth noting that the physiological outcome of JNK activation depends on type of stress, duration of stimuli and the targeted cell type [30]. Similar to JNK, the role of SIRT2 also varies dependent on cell type or stimuli. Studies indicate that SIRT2 inhibition reverses the progression of pathology in neurodegenerative diseases [31]. Similarly, SIRT2 inhibition protects liver against post-ischemic liver injury [18] and hepatic fibrosis [19]. Our results are consistent with these previous findings and SIRT2 inhibition might protect liver against oxidative stress induced by APAP or other stressors. However, SIRT2 inhibition has been shown to promote cell death via p53 activation [32]. FoxO (forkhead box O transcription factor) family of transcription factor has been shown as SIRT2 deacetylase target under oxidative-stress stimuli, thus promoting cell death [16, 33]. Glycolytic enzyme phosphoglycerate mutase has been shown to be deacetylated and activated by SIRT2, as a result of increased ROS, thus promoting cell proliferation and tumour growth [34].

Members of the Sirtuin family are considered as mediators of longevity. Activation of sirtuins delays the development of aging-related diseases [35]. However, the idea of extending longevity by activation of sirtuins seems to be much complex than previously thought. It is interesting to study whether SIRT2 regulates longevity in mammals. Studies conducted in flies, worms and mammals clearly demonstrate that Insulin/IGF/AKT signalling (IIS) promotes aging and aging-related diseases [36]. JNK pathway antagonizes IIS and inhibits IRS1 and AKT, causing nuclear localization and transcriptional activation of FoxO transcription factors to promote longevity [37]. Consistent with our findings, overexpression of Sir2 promotes caspase-dependent apoptosis through activation of JNK in Drosophila. Our previous work and other reports clearly suggest that SIRT1, the closest homologue of the Sir2 gene in *Saccharomyces cerevisiae*, activates insulin signalling (ISS), in contrast to the expectations [29]. The present study shows that SIRT2 could activate JNK and promotes oxidative-stress-induced cell death in HeLa cells. However, the SIRT2-mediated deacetylation of JNK may have different physiological effect depending upon cell type. Chronic deacetylation-dependent hyperactivation of JNK may lead to development of several aging-related diseases like obesity, cancer, muscle degeneration, neurodegeneration and optic atrophy, as JNK is linked to the development of these diseases [2, 5, 38]. Consistent with this hypothesis, studies indicate that inhibition of SIRT2 is beneficial for neurodegenerative diseases and fibrosis [39, 40]. Thus, the physiological or pathological activation of JNK may be linked to the activity of SIRT2 deacetylase. Based on our work, we believe that modulation of SIRT2 might be a potential avenue for treating chronic aging-related diseases in mammals.

Materials and methods

Animal experiments, cell culture and reagents

All animal experiments were carried out with the approval of the Institutional animal ethics committee of Indian Institute of Science, Bengaluru, India constituted as per the

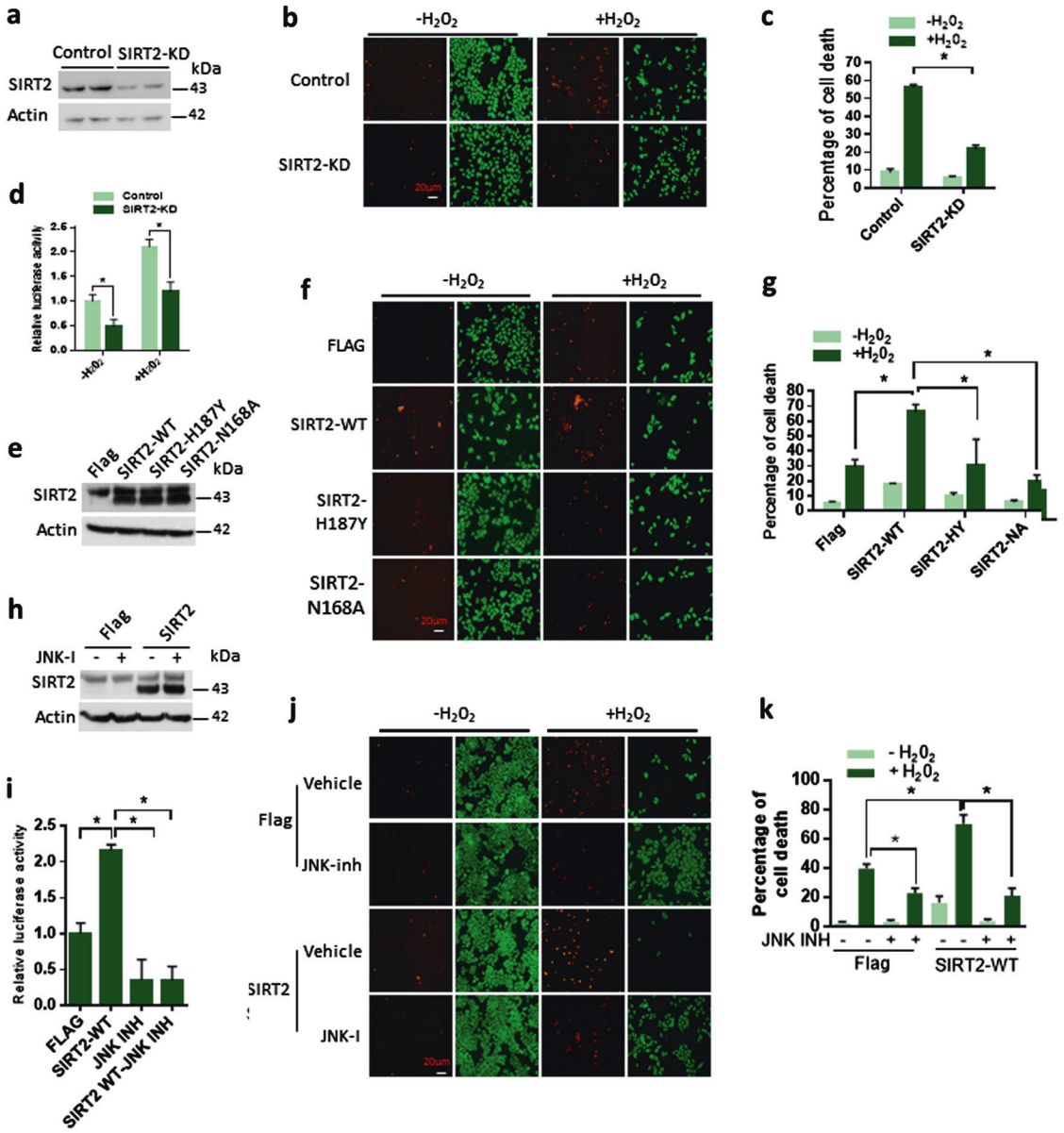

article number 13 of the Committee for Control and Supervision of Experiments on Animals (CPCSEA), Government of India. We performed all animal experiments in accordance with CPCSEA guidelines for animal handling and welfare. Wild-type and SIRT2-KO mice were purchased from Jackson Laboratories, USA, and mice were housed in individual ventilated cages in the clear air facility of Central Animal Facility, Indian Institute of Science. Chow diet and water were given ad libitum. APAP hepatotoxicity experiments were performed as per the standard protocol [41]. Mice were harvested, and liver tissues were fixed immediately in neutral buffered formalin (10%) and preserved until processed further by automated tissue processor (Leica, Germany). Haematoxylin and eosin staining was performed to evaluate the level of degeneration in the liver tissues. TUNEL (terminal deoxinucleotidyl transferase-mediated dUTP-fluorescein nick end labelling) staining was performed using a commercial assay kit (Abcam). Liver function was assessed by measuring the serum aminotransferases by commercial assay kits. HEK 293T and HeLa cell lines were procured from ATCC and cells were cultured at 37 °C, 5% CO_2 in Dulbecco's Modified Eagle Medium supplemented with 10% foetal bovine serum with 100 units/ml penicillin and 100 µg/ml streptomycin. Antibodies were purchased from Sigma Aldrich, Millipore, Santacruz Biotech and Cloud-clone Corp. Plasmids were obtained from Addgene, USA and modified according to the experiment. All reagents, unless specified otherwise, are obtained from Sigma Aldrich. Antibodies used are as follows: Akt1/2/3 (sc-8312), c-Jun (sc-1694), p-

◀ **Fig. 6** SIRT2-dependent deacetylation of JNK regulates H_2O_2-induced cell death in HeLa cells. **a** Western blotting analysis showing the SIRT2 levels in scramble (control) or SIRT2-depleted (SIRT2-KD) HeLa cells. **b** Representative fluorescent microscopic images depicting the H_2O_2-induced cell death in control (scramble) or SIRT2-depleted (SIRT2-KD) HeLa cells. Live (green) and dead (red) were stained after 200 μM H_2O_2 treatment for 12 h. **c** Graph showing the percentage of H_2O_2-induced cell death in control (scramble) or SIRT2-depleted (SIRT2-KD) HeLa cells as measured by the staining for live (Green) and dead (red) cells after 200 μM H_2O_2 treatment for 12 h. $n = 3$ independent experiments. Data are presented as mean ± s.d. $^*p < 0.05$. Two-way ANOVA was used to calculate the *p*-values. **d** Graph showing luciferase reporter assay to analyse JNK activity in control (scramble) or SIRT2-depleted (SIRT2-KD) HeLa cells treated with 200 μM H_2O_2. Reporter plasmid containing multiple binding sites for AP-1 was used to track the activity of JNK in HeLa cells. $n = 3$ independent experiments. Data are presented as mean ± s.d. $^*p < 0.05$. Two-way ANOVA was used to calculate the *p*-values. **e** Western blotting analysis showing the SIRT2 levels in HeLa cells over-expressing either Flag, wild-type and mutant versions of SIRT2. **f** Representative fluorescent microscopic images depicting the H_2O_2-induced cell death in HeLa cells overexpressing either Flag, wild-type and mutant versions of SIRT2. Live (green) and dead (red) were stained after 200 μM H_2O_2 treatment for 12 h. **g** Graph showing the percentage of H_2O_2-induced cell death in HeLa cells overexpressing either Flag, wild-type and mutant versions of SIRT2, as measured by the staining for live (Green) and dead (red) cells after 200 μM H_2O_2 treatment for 12 h. $n = 3$ independent experiments. Data are presented as mean ± s.d. $^*p < 0.05$. Two-way ANOVA was used to calculate the *p*-values. **h** Western blotting analysis showing the SIRT2 levels in Flag or wild-type SIRT2 overexpressing HeLa cells treated with JNK inhibitor (JNK-I). **i** Graph showing luciferase reporter assay to analyse JNK activity in Flag or wild-type SIRT2 overexpressing HeLa cells treated with JNK inhibitor (JNK-I). Reporter plasmid containing multiple binding sites for AP-1 was used to assess the activity of JNK in HeLa cells. $n = 3$ independent experiments. Data are presented as mean ± s.d. $^*p < 0.05$. One-way ANOVA was used to calculate the *p*-values. **j** Representative fluorescent microscopic images depicting the H_2O_2-induced cell death in Flag or wild-type SIRT2 overexpressing HeLa cells treated with JNK inhibitor (JNK-I). Live (green) and dead (red) were stained after 200 μM H_2O_2 treatment for 12 h. **k** Graph showing the percentage of H_2O_2-induced cell death in Flag or wild-type SIRT2 overexpressing HeLa cells treated with JNK inhibitor (JNK-I), as measured by the staining for live (Green) and dead (red) cells after 200 μM H_2O_2 treatment for 12 h. $n = 3$ independent experiments. Data are presented as mean ± s.d. $^*p < 0.05$. Two-way ANOVA was used to calculate the *p*-values

c-Jun (sc-822), GAPDH (sc-25778), JNK (sc-571), p-JNK (sc-6254) from Santacruz Biotech, DUSP1, DUSP3, DUSP6 from Cloud-Clone Corp. Ac-Lys (9681), p-Akt (Ser473; 4060), p-Akt (Thr308; 13038), c-Jun Fusion (6093), p-JNK (9251), SIRT2 (12650), β-Actin (12262) from Cell signaling, Acetyl Lysine (06-933), JNK (2470917), p300 (2328343), p-JNK (3049) from Millipore, MKK4, DUSP4 and p-MKK4 are from Thermo Fisher Scientific. Secondary Rabbit anti-Mouse (sc-2005) and Goat anti-Rabbit (sc-2004) used are from Santacruz. Plasmids and adenoviruses used are as follows: PCAF, p300, GST-JNK, Flag-JNK1, GFP-JNK1, Flag-SIRT2, p300-shRNA-expressing adenovirus, SIRT2 adenovirus, and Null Adenovirus. shRNA for CBP, PCAF, p300, GCN5 and TIP60 are from sigma shRNA library. For all the adenovirus experiment,s viruses were used at a multiplicity of infection of 10. SIRT2 adenovirus was purchased from Vector Biolabs. Adenovirus vectors synthesizing shRNA against p300 and luciferase were kindly provided by B. Thimmapaya, Northwestern University, Chicago, USA. Full-length JNK1, p300, PCAF and SIRT2 genes were cloned in Flag or HA-tagged vectors. Transfection was performed using Lipofectamine 2000 transfection reagent (Invitrogen, USA) as per the manufacturer's instructions. For generating stable knockdown, oligonucleotide sequences were designed and cloned in pLKO.1 vector. The insert was confirmed by agarose gel electrophoresis and sequencing (SciGenom). QuickChange Primer Design tool was used to design primers to introduce point mutations into the DNA sequences of SIRT2 and JNK. Site-directed mutagenesis was carried out as per previously described protocol [42]. The results were verified by sequencing (SciGenom).

Modelling and molecular dynamics simulations

Crystal structure of JNK (PDB ID 4QTD, resolution 1.5 Å) was used to generate the initial model for the wild-type JNK. Ligands SCH772984 and triphosphate seen in the pocket of JNK was replaced with the ATP molecule. The model was overlaid on the structure of ATP-bound JNK (PDB ID 4UX9, resolution 2.34 Å) to confirm the conformation of ATP ligand in the binding pocket. Computer-aided acetylation (acK153) was done using the PyTMs plugin of PyMOL [43]. UCSF Chimera software package was used to generate JNK-K153R mutant on the initial model of JNK wild type as template [44]. The modelled structure of JNK-153R was further energy minimized in GROMACS using steepest descent energy minimization until the system converged with Fmax no greater than 1000 kJ/mol/nm. In the final energy-minimized structure, the side chain of R153 adopts a conformation (with χ1 64.4°, χ2 −170.5°, χ3 70.2°, χ4 −174.8°) that matches well with the side chain conformation of K153 (χ1 67.2°, χ2 −168.5°, χ3 79.3°, χ4 −178.7°) in wild-type JNK. UCSF Chimera software package was used for visualization, analysis and generation of final images [43].

GROMACS simulation package, version 5.0.4 was used to run MD simulations on the initial models generated for the wild-type and acetylated mutant of JNK. Parameterization was performed using CHARMM27 force field with CMAP correction and rigid water model [45]. Each model was placed in dodecahedron box containing TIP3P water with a minimum distance of 10 Å between the protein atom and box surface. Counter ions Na^+ and Cl^- were added for charge neutralization. Steepest descent energy minimization was performed until the system converged

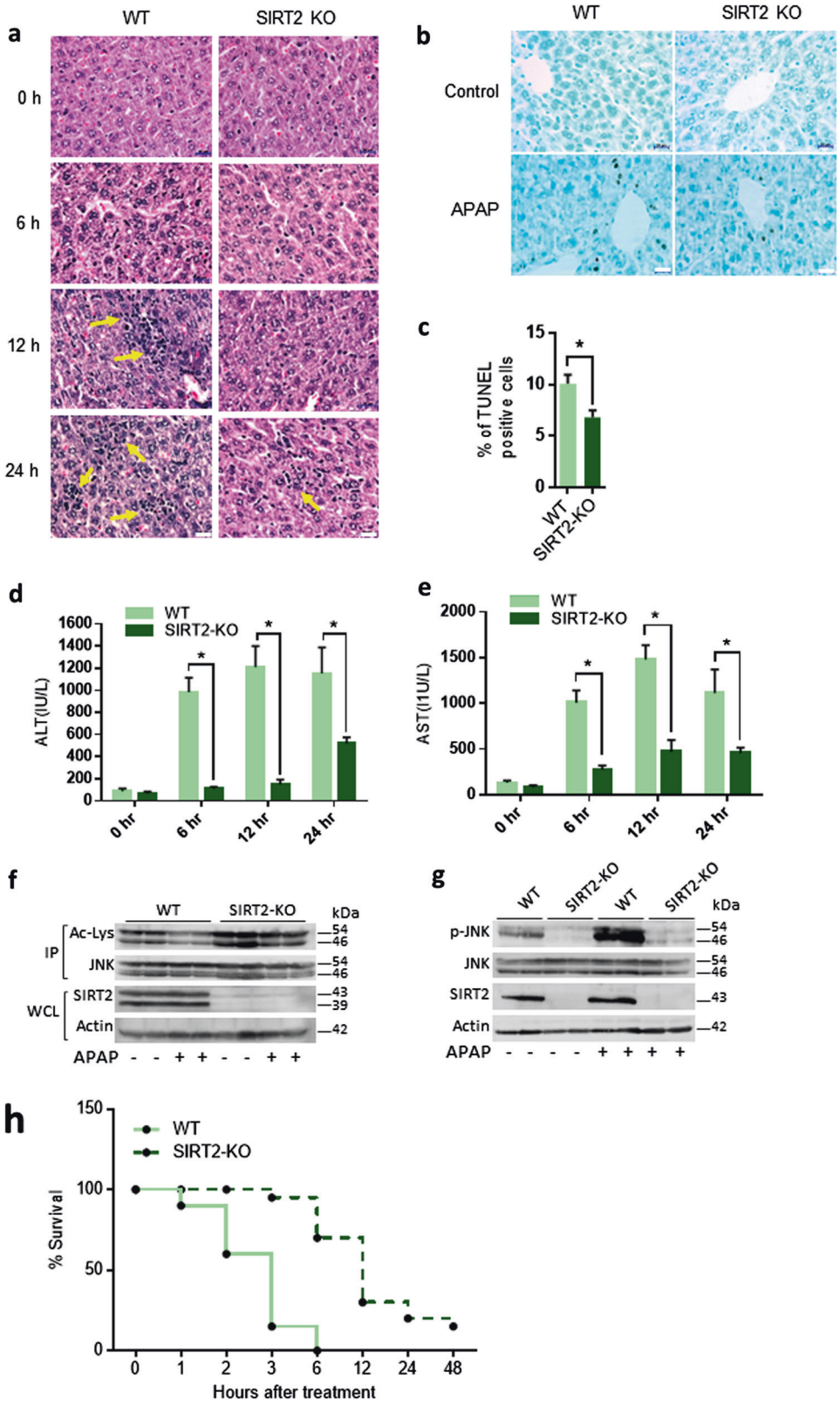

with Fmax no greater than 1000 kJ/mol/nm. Both the systems were sufficiently equilibrated for 1.2 ns under NVT and 2.4 ns under NPT ensemble, while coupling protein, ATP, ions and water separately. A constant temperature of 300 K was maintained by coupling the v-rescale thermostat at 0.1 ps. Berendsen thermostat was used to maintain the

◀ **Fig. 7** SIRT2 deficiency prevents acetaminophen (APAP)-induced liver cell death. **a** Representative H&E staining images of wild-type (WT) and SIRT2-deficient (SIRT2-KO) mice liver sections showing degenerative changes (arrows) when injected with 100 mg/kg APAP intraperitoneally. SIRT2-KO mice show reduced degenerative changes. $n = 5$ mice per group/time point. Scale bar = 20 μM. **b** Representative TUNEL staining images of WT and SIRT2-KO mice liver sections showing TUNEL-positive cells (brown nuclei) 24 h post injection with 100 mg/kg APAP intraperitoneally. $n = 5$ mice per group. **c** Graph showing the percentage of TUNEL-positive cells in WT and SIRT2-KO mice liver sections. Mice were sacrificed 24 h post 100 mg/kg APAP intraperitoneal injection. $n = 5$ mice per group. Scale bar = 20 μM Data are presented as mean ± s.d. $*p < 0.05$. Student's *t*-test was used to calculate the *p*-values. **d** Graph depicting the levels of serum alanine aminotransferase (ALT) in WT and SIRT2-KO mice. Mice were sacrificed at different time points after 100 mg/kg acetaminophen (APAP) intraperitoneal injection. $n = 5$ mice per group. Data are presented as mean ± s.d. $*p < 0.05$. Two-way ANOVA was used to calculate the *p*-values. **e** Graph depicting the levels of serum aspartate aminotransferase (AST) in WT and SIRT2-KO mice. Mice were sacrificed at different time points after 100 mg/kg APAP intraperitoneal injection. $n = 5$ mice per group. Data are presented as mean ± s.d. $*p < 0.05$. Two-way ANOVA was used to calculate the *p*-values. **f** Western blotting images depicting the acetylation of endogenous JNK in the liver lysates of WT and SIRT2-KO mice injected with vehicle or 100 mg/kg APAP. JNK was immunoprecipitated and assessed for the acetylation of JNK. Whole cell lysates (WCLs) were probed for the protein levels of SIRT2 by western blotting. **g** Western blotting images depicting the phosphorylation of endogenous JNK in the liver lysates of WT and SIRT2-KO mice injected with vehicle or 100 mg/kg APAP. WCLs were probed for phosphorylation of JNK and total protein levels of SIRT2 by western blotting. **h** Graph showing the survival of WT and SIRT2-KO mice injected with high dose of APAP (600 mg/kg; APAP). $n = 20$ mice per group

pressure of the bath at 1 bar with a 1 ps coupling constant. The electrostatic interactions were evaluated using the Particle Mesh Ewald method [46]. A 2-fs integration time step was used for the production run of each simulation. Two independent trajectories of 50 ns each were then performed upon the equilibrated systems using leap-frog algorithm.

GROMACS tools were used to calculate the RMSD of Cα atoms, RMSD of ATP nucleotide and the resultant RMSF of Cα atoms on the two MD trajectories of 50 ns each for both the wild-type and the acK151 mutant of JNK. UCSF Chimera software tool was used for visualization and calculation of distances between the atoms.

List of primers for site-directed mutations in JNK1, SIRT2 and oligonucleotide sequences for stable knockdown generation

Jnk1 K30Q: For 5′gagcctataggctgtaaattctgatatcg3′, Rev 5′cgatatcagaatttacagcctataggctc3′; Jnk1 K153Q: For 5′ctgggctgtaagtcccgatgaataattcc3′, Rev5′ggaattattcatcgggac ttacagcccag3′; Jnk1 K160Q: For 5′gcaatcagactgtactactata ttactggg3′, Rev 5′cccagtaatatagtagtacagtctgattgc3′; Jnk1 K166Q: For 5′catctacagagatcctctgagatgcatctattaccagcattttgg ataac3′, Rev5-gtaaaatctgattgcactttgcagattcttgacttcggtctgg3′; Jnk1 K265Q: For 5′gctatatccagcatactgaggtctgttttc3′, Rev 5′ gaaaacagacctcagtatgctggatatagc3′; Jnk1 K308Q: For 5′cca-gaccgaagtcaagaatctgcaaagtgcaatcagattttac3′, Rev 5′gttatc-caaaatgctggtaatagatgcatctcagaggatctctgtagatg3′; Jnk1K30R: For 5′ctgagcctataggtcttaaattctgatatcgtttcaggactg3′, Rev 5′ cagtcctgaaacgatatcagaatttaagacctataggctcag3′; Jnk1K153R: For 5′ctatattactgggccttaagtcccgatgaataattccagca3′, Rev 5′ tgctggaattattcatcgggacttaaggcccagtaatatag3′; Jnk1K160R: For 5′gaatcttcaaagtgcaatcagatcttactactatattactgggctttaa3′, Rev 5′ttaaagcccagtaatatagtagtaagatctgattgcactttgaagattc3′; Jnk1 K166R: For 5′tctacagagatccttctagatgcatctattaccagcatttt gga3′, Rev 5′aaaatctgattgcactttgaggattcttgacttcggtctgg3′; Jnk1K265R: For 5′ctcaaagctatatccagcatatctaggtctgttttcaa cgtaagt3′, Rev 5′acttacgttgaaaacagacctagatatgctggatatagcttt gag3′; Jnk1 K308R: For 5′tccaaaatgctggtaatagatgcatctag aaggatctctgtaga3′, Rev 5′ccagaccgaagtcaagaatcctcaaagtgcaa tcagatttt3′; Sirt2 N168A: For 5′ctccagggtatctatggcctgcgtg-tagcagcgc3′, Rev 5′gcgctgctacacgcaggccatagatacccctggag3′; Sirt2 H187Y: For 5′atgtgtagaaggtgccatacgcctccaccaagtcc3′, Rev 5′ggacttggtggaggcgtatggcaccttctacacat3′. JNK shRNA1—5′tctggtatgatccttctgaa3′, JNK shRNA2—5′caagggattt gttatccaaa3′, JNK shRNA3—5′actcagaacacaacaaacttt3′, SIRT2 shRNA1—5′ gaggccatctttgagatca 3′, SIRT2 shRNA2—5′ atgacaacctagagaagta 3′, Scrambled—5′ ggtggaaa-gactgaaatatgt 3′.

List of real-time quantitative PCR (qPCR) primers

Mkk4: For 5′agtggacagcttgtggactct3′, Rev 5′aactccaga-catcagagcgga3′; Mkk7: For 5′tccagatcccaccaagcctgactatg3′, Rev 5′aatgactggaagtcccctgagaagcc3′; MAP3K4: For 5′ ctaagtcctatgataacgtcatgc3′, Rev 5′tgaaatcgaatctccttcatgg3′; MAP3K10: For 5′ctggtgatggaatatatgctcg3′, Rev 5′ccaggat-taggatgttgatgg3′; MAP3K11: For 5′cccttcaactctgaatc-taatcc3′, Rev 5′cgaagtggatctacttgaagc3′; MAP3K7: For 5′ actcacttgatgcggt3′, Rev 5′cggcgatcctagcttc3′, JNK1: For 5′ ccagtcaggcaagggattt3′, Rev 5′cgatgatgatgatggatgctgagag3′; JNK2: For 5′acaccatccgcagagttcat3′, Rev 5′caaggcttcgtcca-cagaga3′; JNK3: For 5′aaccagttcctacagtgtggaagtg3′, Rev 5′ ctgaatcacttgacataagttggc3′; CBP: For 5′agttcccgtcatccagcg3′, Rev 5′aggccccagcatgttgag3′; GCN5: For 5′ ttccgagtgga-gaaggaca3′, Rev 5′ agcatggacaggaatttgg3′; TIP60: For 5′ agcgtcatttgaccaagtgt3′, Rev 5′ agttcatagctgaactcgat3′.

RNA extraction and real-time qPCR reaction

Protocols for RNA extraction and real-time qPCR reaction was described in our recent works [29, 47]. RNA was extracted using TRIZOL reagent (Thermo Fisher) and further processed to synthesize first strand of cDNA according to the manufacturer's protocol. The qPCR reaction was set

up in Bio-Rad CFX 384 instrument with the following loop —[95 °C (10 s), 60 °C (40 s), 72 °C (25 s)] × 40. The experiment was done in three replicates and the data were normalized using actin as housekeeping gene.

Immunoblotting and immunoprecipitation

Protocols for immunoblotting and immunoprecipitation are described in our previous works [29, 48]. Transfected cells were harvested after washing with ice-cold phosphate-buffered saline (PBS) and lysed in an ice-cold lysis buffer (20 mM Tris-Cl, 150 mM NaCl, 1% Triton X-100, 1 mM EDTA, 1 mM EGTA, 2.5 mM sodium pyrophosphate, 1 mM Na_3VO_4, protease inhibitor cocktail (Roche)). Bradford reagent (BIO-RAD # 500-006) was used to perform protein quantification. Equal amount of protein from cell lysate was mixed with Laemmli Buffer (2×, BioRad) in a 1:1 ratio, boiled for 5 min and resolved by sodium dodecyl sulphate-polyacrylamide gel electrophoresis (SDS-PAGE) followed by overnight transfer to a polyvinylidene difluoride (PVDF) membrane (GE, #10600023) at 25 V. For immunoprecipitation, 500 µg of protein from cell lysate was incubated with the appropriate antibody overnight. The immune complexes were collected using Protein A/G-agarose beads (Sigma, USA). The immunoprecipitated protein was resolved by SDS-PAGE and transferred to a PVDF membrane (GE, #10600023). The membranes were blocked with a solution of 5% non-fat dried milk in TBST buffer (25 mM Tris-HCl, pH 7.5, 150 mM NaCl, 0.05% Tween 20). For detection of respective proteins, blots were incubated with primary antibody (Santa Cruz Biotechnology, Cell Signaling or Millipore; 1:1000) at 4 °C overnight. Non-specifically bound primary antibody was removed by washing three times with TBST buffer followed by peroxidase-conjugated secondary antibody (Santa Cruz, 1:10,000) incubation at room temperature for 1 h. Non-specifically bound secondary antibody was removed by washing the blot three times with TBST buffer. Signals were detected using chemiluminescence substrate solution (Thermo fisher # 34080) and analysed by a GE LAS4000 luminescent image analyser .

Protein purification

GST-JNK1 expression plasmid was transformed into competent *Escherichia coli* BL21 (DE3) cells. Single colony was inoculated in LB medium at 37 °C in orbital shaker incubator till mid log phase. IPTG (50 µM) was added to the culture and incubated at 18 °C for 18 h. Following incubation, the culture was centrifuged at 2300 × *g* for 10 min at 4 °C, and the resulting pellet was resuspended in binding buffer (50 mM Tris-Cl, pH 8.0, 150 mM NaCl, 1 mM PMSF (Sigma)). Cells were lysed by sonication and centrifuged at 12,000 × *g* for 30 min at 4 °C. After centrifugation, supernatant was collected and incubated with Ni-NTA agarose beads and kept for agitation for overnight at 4 °C. After overnight binding, beads were washed with wash buffer (150 mM NaCl, 50 mM Tris-Cl, pH 7.5, 1% Triton X 100) and bead-bound protein was eluted and stored in 30% glycerol containing buffer.

In vitro JNK1 acetylation assay

Protocols for in vitro acetylation assays are described in our previous works [29, 48]. Recombinant JNK protein was expressed in *E. coli* BL21 (DE3) and purified by affinity chromatography. Purified JNK protein was incubated with p300 acetyltransferase (Millipore # 2273152) and PCAF (Millipore # 14-309) for 2 h. GST-JNK bound beads were washed three times with HAT buffer (50 mM Tris-Cl, pH 8.0, 1 mM EDTA, 10 mM Na-butyrate, 5 mM DTT, 10 mM NaCl and 10% glycerol). Beads bound to JNK were incubated with 1 µg of acetyltransferase (p300 or PCAF) in 50 µl of HAT buffer supplemented with 100 µM acetyl CoA. Samples were incubated at 30 °C for 2 h. Beads were washed 3 times with TBS and protein was eluted by adding 50 µl of sample buffer (125 mM Tris-Cl, pH 6.8, with 4% SDS, 20% (v/v) glycerol and 0.004% bromophenol blue). Samples were heated for 5 min at 95 °C followed by centrifugation at 13,400 × *g*, 30 s and supernatant were subjected to SDS-PAGE. JNK acetylation was detected with pan anti-acetyl Lysine antibody (Cell Signaling #9681).

In vitro JNK1 deacetylation and activity assay

Protocols for deacetylation assays are described in our previous works [29, 48]. Cells at ~70% confluence were transfected with Flag-Sirt2 expression plasmid. Twenty four hours after transfection, the cells were harvested after washing with ice-cold PBS and lysed in an ice-cold lysis buffer [50 mM Tris-Cl, pH 7.4, 150 mM NaCl, 1 mM EDTA, 1% Triton X-100 and protease inhibitor cocktail (Sigma Aldrich)] followed by vortexing for 15 s at 5 min interval for 30 min and centrifuged at 13,400 × *g*, 10 min, 4°C. After centrifugation, supernatant was collected, and 500 µg of total protein was incubated with 50 µl agarose beads conjugated to Anti-Flag antibody (Sigma A2220) and kept for agitation for 2 h at 4 °C. Beads were centrifuged for 30 s, 100 × *g*, 4°C and washed with 0.5 ml of TBS (25 mM Tris-HCl, pH 7.5, 150 mM NaCl) 3 times and used for in vitro deacetylation assay. On the other hand, Flag-JNK1 expression plasmid was transfected into cells. Twenty four hours after transfection, 500 µg of total protein was incubated with 50 µl agarose beads bound anti-Flag antibody (Sigma A2220) and kept for agitation for 2 h at 4 °C. Beads were centrifuged for 30 s, 100 × *g*, 4 °C and washed with 0.5 ml of TBS 3 times and beads bound to JNK1 protein

were incubated with previously isolated SIRT2 protein in deacetylation buffer (250 mM Tris-Cl, pH 9.0, 20 mM $MgCl_2$, 250 mM NaCl, 2.5 mM DTT, 5 mM NAD^+, 2.5 μM TSA) for 2 h at 30°C. Following deacetylation, flag-JNK1 was washed 3 times with kinase buffer (25 mM Tris-Cl, pH 7.5, 10 mM $MgCl_2$, 5 mM β-glycerophosphate, 0.1 mM Na_3VO_4, 2 mM DTT) and incubated with 200 μM ATP and 250 μg/ml c-Jun fusion protein in kinase buffer (total volume 50 μl) for 30 min at 30 °C, and reaction was terminated by adding 2×Laemmli Sample Buffer (Bio-Rad). Western blotting was performed, and the level of c-Jun phosphorylation was detected by primary antibody against phospho c-Jun.

ATP-binding assay

Filter binding assay for ATP binding to JNK and mutated JNK at position K153Q and K153R was performed by incubating with [γ ^{32}P] ATP (2 μCi) at 30 °C for 10 min in (20 mM HEPES pH 7.5, 50 mM NaCl, 10 mM $MgCl_2$, 2 mM $CaCl_2$, 200 μM ATP) in a final volume of 20 μL. After 30 min, the entire reaction was loaded on nitrocellulose paper (Sigma) and the membrane was dried. This was followed by three washes using the same binding buffer to remove unbound ATP. Dry nitrocellulose filters were put into scintillation vials, and the radioactivity was measured using a scintillation counter (Beckman).

Luciferase reporter assay

The cells were transfected with plasmid harbouring activating protein-1 (AP-1) luciferase reporter element using Lipofectamine 2000 (Invitrogen), and standard protocol was followed to perform the assay. A luminometer was used to measure the luminescence (Pharmingen Moonlight 3010; BD Biosciences, San Jose, CA, USA).

Confocal microscopy

Confocal microscopy was performed as described previously [49, 50]. Cells were washed with 1× PBS and fixed using 4% paraformaldehyde in PBS for 10 min at room temperature. After fixing the cells, samples were incubated for 10 min with PBS containing 0.25% Triton X-100. Samples were blocked with 1% bovine serum albumin (BSA) prepared in PBST (PBS with 1% Tween 20) containing glycine (22.52 mg/ml) for 30 min. Following blocking, samples were incubated with primary antibody overnight at 4 °C. Primary antibody was removed by washing 3 times for 5 min each with PBS. Cells were incubated with secondary antibody in 1% BSA for 1 h at room temperature in the dark. Secondary antibody was discarded, and cells were washed 3 times with PBS for 5 min each. Coverslip was mounted using Molecular Probes mounting medium (P36935), and images was taken at 40× or 63× magnification using Zeiss LSM 880 Airyscan Confocal Microscope.

Live/dead cell assay

Cells were plated in duplicates in 60 mm dish and were treated with either vehicle or H_20_2 for 12 h at 80% confluency. Following this, cells were stained with Live/dead cell assay reagent in PBS for 30 min at room temperature according to the manufacturer's protocol (Live/Dead Kit for Mammalian Cells, #L3224, Thermo Scientific). Live cells stained green (Calcein-AM), whereas dead cells stained red (Ethidium homodimer-1). Cells were visualized by Olympus 1×2-UCB fluorescence microscope. In all experiments, 400–500 cells per group was counted for quantification.

MTT (3-[4,5-dimethylthiazol-2-yl]-2,5 diphenyl tetrazolium bromide) assay

Cells were plated on 24-well plate. In all experiments, 20 μl of MTT (5 mg/ml) reagent was added and incubated for 2–4 h. Media was discarded and 110 μl of dimethyl sulphoxide was added and mixed twice. In all experiments, 100 μl from each well was transferred to 96-well plate. Reading was taken at 570 nm using VERSA max microplate reader, Molecular Devices.

Statistical analysis

All experiments were at least done in independent triplicates. Data were analysed using statistics module in MS Excel 2013 or Graph Pad Prism version 6.04. Data in bar graphs are represented in the form of mean ± standard deviation. Densitometric analysis for immunoblots were performed and analysed using the ImageJ software. The fold change was presented as absolute number in the respective figures.

Acknowledgements We thank Meisam Bagheri and Prof. Deepak K. Saini for helping in liver function tests. Adenovirus vectors synthesizing shRNA against p300 and luciferase were kindly provided by Prof. B. Thimmapaya, Northwestern University, Chicago, USA. We thank Venkataraman Ravi, Danish Khan, Anwit S. Pandit, Aditi Jain and Shweta Kumar for technical support and for critical inputs for the manuscript.

Author contributions All the experiments, except MS/MS analysis, listed in the manuscript were performed at the Indian Institute of Science, Bengaluru, India. MS performed most of the experiments. SM performed confocal microscopy and wrote the first draft of the manuscript. CK and MS performed molecular modelling and molecular dynamic simulations. PAS performed histological analysis. DW and MPG performed mass spectrometric analysis. NRS conceived the study, designed experiments, coordinated with investigators and wrote the final version of the manuscript.

Funding NRS is the recipient of Ramalingaswami Re-entry Fellowship and the Innovative Young Biotechnologist Award (IYBA) from the Department of Biotechnology, Government of India. PAS is an Inspire-Faculty fellow. NRS's laboratory is supported by research funding from Department of Science and Technology (EMR/2014/000065), the Department of Biotechnology (BRB/10/1294/2014 and MED/30/1454/2014), the Council for Scientific and Industrial Research (37(1646)/15/EMR-II) and the Department of Biotechnology–Indian Institute of Science partnership program for advanced research.

Compilance with ethical standards

Conflict of interest The authors declare that they have no conflict of interest.

References

1. Gupta S, Barrett T, Whitmarsh AJ, Cavanagh J, Sluss HK, Derijard B, et al. Selective interaction of JNK protein kinase isoforms with transcription factors. EMBO J. 1996;15:2760–70.
2. Ip YT, Davis RJ. Signal transduction by the c-Jun N-terminal kinase (JNK)--from inflammation to development. Curr Opin Cell Biol. 1998;10:205–19.
3. Davis RJ. Signal transduction by the JNK group of MAP kinases. Cell. 2000;103:239–52.
4. Moriguchi T, Toyoshima F, Masuyama N, Hanafusa H, Gotoh Y, Nishida E. A novel SAPK/JNK kinase, MKK7, stimulated by TNFalpha and cellular stresses. EMBO J. 1997;16:7045–53.
5. Wagner EF, Nebreda AR. Signal integration by JNK and p38 MAPK pathways in cancer development. Nat Rev Cancer. 2009;9:537–49.
6. Xia ZG, Dickens M, Raingeaud J, Davis RJ, Greenberg ME. Opposing effects of Erk and Jnk-P38 MAP kinases on apoptosis. Science. 1995;270:1326–31.
7. Tournier C, Hess P, Yang DD, Xu J, Turner TK, Nimnual A, et al. Requirement of JNK for stress-induced activation of the cytochrome c-mediated death pathway. Science. 2000;288:870–4.
8. Kim SM, Park JH, Chung SK, Kim JY, Hwang HY, Chung KC, et al. Coxsackievirus B3 infection induces cyr61 activation via JNK to mediate cell death. J Virol. 2004;78:13479–88.
9. Maldonado E, DeHart DN, Fang D, Heslop K, Gooz MB, Lemasters J. Oxidative stress and JNK activation cause mitochondrial dysfunction and cell death in hepatocarcinoma after VDAC-tubulin antagonists. Biophys J. 2016;110:470a–470a.
10. Xie Y, McGill MR, Dorko K, Kumer SC, Schmitt TM, Forster J, et al. Mechanisms of acetaminophen-induced cell death in primary human hepatocytes. Toxicol Appl Pharmacol. 2014;279:266–74.
11. Saito C, Lemasters JJ, Jaeschke H. c-Jun N-terminal kinase modulates oxidant stress and peroxynitrite formation independent of inducible nitric oxide synthase in acetaminophen hepatotoxicity. Toxicol Appl Pharmacol. 2010;246:8–17.
12. Choudhary C, Weinert BT, Nishida Y, Verdin E, Mann M. The growing landscape of lysine acetylation links metabolism and cell signalling. Nat Rev Mol Cell Biol. 2014;15:536–50.
13. Inoue T, Hiratsuka M, Osaki M, Yamada H, Kishimoto I, Yamaguchi S, et al. SIRT2, a tubulin deacetylase, acts to block the entry to chromosome condensation in response to mitotic stress. Oncogene. 2007;26:945–57.
14. North BJ, Marshall BL, Borra MT, Denu JM, Verdin E. The human Sir2 ortholog, SIRT2, is an NAD+-dependent tubulin deacetylase. Mol Cell. 2003;11:437–44.
15. Park SH, Zhu YM, Ozden O, Kim HS, Jiang HY, Deng CX, et al. SIRT2 is a tumor suppressor that connects aging, acetylome, cell cycle signaling, and carcinogenesis. Transl Cancer Res. 2012;1:15–21.
16. Wang F, Nguyen M, Qin FXF, Tong Q. SIRT2 deacetylates FOXO3a in response to oxidative stress and caloric restriction. Aging Cell. 2007;6:505–14.
17. Lynn EG, McLeod CJ, Gordon JP, Bao JJ, Sack MN. SIRT2 is a negative regulator of anoxia-reoxygenation tolerance via regulation of 14-3-3 zeta and BAD in H9c2 cells. FEBS Lett. 2008;582:2857–62.
18. Wang J, Koh HW, Zhou L, Bae UJ, Lee HS, Bang IH, et al. Sirtuin 2 aggravates postischemic liver injury by deacetylating mitogen-activated protein kinase phosphatase-1. Hepatology. 2017;65:225–36.
19. Arteaga M, Shang N, Ding X, Yong S, Cotler SJ, Denning MF, et al. Inhibition of SIRT2 suppresses hepatic fibrosis. Am J Physiol Gastrointest Liver Physiol. 2016;310:G1155–1168.
20. Mizukami Y, Yoshioka K, Morimoto S, Yoshida K. A novel mechanism of JNK1 activation. Nuclear translocation and activation of JNK1 during ischemia and reperfusion. J Biol Chem. 1997;272:16657–62.
21. Daitoku H, Hatta M, Matsuzaki H, Aratani S, Ohshima T, Miyagishi M, et al. Silent information regulator 2 potentiates Foxo1-mediated transcription through its deacetylase activity. Proc Natl Acad Sci USA. 2004;101:10042–7.
22. Liu J, Lin AN. Role of JNK activation in apoptosis: a double-edged sword. Cell Res. 2005;15:36–42.
23. Dhanasekaran DN, Reddy EP. JNK signaling in apoptosis. Oncogene. 2008;27:6245–51.
24. Singh M, Sharma H, Singh N. Hydrogen peroxide induces. apoptosis in HeLa cells through mitochondrial pathway. Mitochondrion. 2007;7:367–73.
25. Park WH. The effect of MAPK inhibitors and ROS modulators on cell growth and death of H2O2-treated HeLa cells. Mol Med Rep. 2013;8:557–64.
26. Gunawan BK, Liu ZX, Han D, Hanawa N, Gaarde WA, Kaplowitz N. c-Jun N-terminal kinase plays a major role in murine acetaminophen hepatotoxicity. Gastroenterology. 2006;131:165–78.
27. Win S, Than TA, Han D, Petrovic LM, Kaplowitz N. c-Jun N-terminal kinase (JNK)-dependent acute liver injury from acetaminophen or tumor necrosis factor (TNF) requires mitochondrial Sab protein expression in mice. J Biol Chem. 2011;286:35071–8.
28. Tang Y, Zhao WH, Chen Y, Zhao YM, Gu W. Acetylation is indispensable for p53 activation. Cell. 2008;133:612–26.
29. Sundaresan NR, Pillai VB, Wolfgeher D, Samant S, Vasudevan P, Parekh V, et al. The deacetylase SIRT1 promotes membrane localization and activation of Akt and PDK1 during tumorigenesis and cardiac hypertrophy. Sci Signal. 2011;4:ra46.
30. Kuan CY, Yang DD, Roy DRS, Davis RJ, Rakic P, Flavell RA. The Jnk1 and Jnk2 protein kinases are required for regional specific apoptosis during early brain development. Neuron. 1999;22:667–76.
31. Herskovits AZ, Guarente L. Sirtuin deacetylases in neurodegenerative diseases of aging. Cell Res. 2013;23:746–58.
32. Lain S, Hollick JJ, Campbell J, Staples OD, Higgins M, Aoubala M, et al. Discovery, in vivo activity, and mechanism of action of a small-molecule p53 activator. Cancer Cell. 2008;13:454–63.
33. Wang Y, Mu Y, Zhou X, Ji H, Gao X, Cai WW, Guan Q, Xu T. SIRT2-mediated FOXO3a deacetylation drives its nuclear translocation triggering FasL-induced cell apoptosis during renal ischemia reperfusion. Apoptosis. 2017; 22:519–530.
34. Xu Y, Li F, Lv L, Li T, Zhou X, Deng CX, et al. Oxidative stress activates SIRT2 to deacetylate and stimulate phosphoglycerate mutase. Cancer Res. 2014;74:3630–42.
35. Haigis MC, Sinclair DA. Mammalian sirtuins: biological insights and disease relevance. Annu Rev Pathol. 2010;5:253–95.

36. Salminen A, Kaarniranta K. Insulin/IGF-1 paradox of aging: regulation via AKT/IKK/NF-kappa B signaling. Cell Signal. 2010;22:573–7.
37. Oh SW, Mukhopadhyay A, Svrzikapa N, Jiang F, Davis RJ, Tissenbaum HA. JNK regulates lifespan in *Caenorhabditis elegans* by modulating nuclear translocation of forkhead transcription factor/DAF-16. Proc Natl Acad Sci USA. 2005;102:4494–9.
38. Seki E, Brenner DA, Karin M. A liver full of JNK: signaling in regulation of cell function and disease pathogenesis, and clinical approaches. Gastroenterology. 2012;143:307–20.
39. Luthi-Carter R, Taylor DM, Pallos J, Lambert E, Amore A, Parker A, et al. SIRT2 inhibition achieves neuroprotection by decreasing sterol biosynthesis. Proc Natl Acad Sci USA. 2010;107:7927–32.
40. Ponnusamy M, Zhou XX, Yan YL, Tang JH, Tolbert E, Zhao TC, et al. Blocking sirtuin 1 and 2 inhibits renal interstitial fibroblast activation and attenuates renal interstitial fibrosis in obstructive nephropathy. J Pharmacol Exp Ther. 2014;350:243–56.
41. Kim YH, Hwang JH, Kim KS, Noh JR, Choi DH, Kim DK, et al. Metformin ameliorates acetaminophen hepatotoxicity via Gadd45beta-dependent regulation of JNK signaling in mice. J Hepatol. 2015;63:75–82.
42. Zheng L, Baumann U, Reymond JL. An efficient one-step site-directed and site-saturation mutagenesis protocol. Nucleic Acids Res. 2004;32:e115.
43. Warnecke A, Sandalova T, Achour A, Harris RA. PyTMs: a useful PyMOL plugin for modeling common post-translational modifications. BMC Bioinformatics. 2014;15:370.
44. Pettersen EF, Goddard TD, Huang CC, Couch GS, Greenblatt DM, Meng EC, et al. UCSF Chimera--a visualization system for exploratory research and analysis. J Comput Chem. 2004;25:1605–12.
45. Jorgensen WL, Chandrasekhar J, Madura JD, Impey RW, Klein ML. Comparison of simple potential functions for simulating liquid water. J Chem Phys. 1983;79:926–35.
46. Darden T, York D, Pedersen L. Particle mesh Ewald - an N.Log (N) method for Ewald sums in large systems. J Chem Phys. 1993;98:10089–92.
47. Khan D, Sarikhani M, Dasgupta S, Maniyadath B, Pandit AS, Mishra S, et al. SIRT6 deacetylase transcriptionally regulates glucose metabolism in heart. J Cell Physiol. 2018. https://doi.org/10.1002/jcp.26434.
48. Sundaresan NR, Vasudevan P, Zhong L, Kim G, Samant S, Parekh V, et al. The sirtuin SIRT6 blocks IGF-Akt signaling and development of cardiac hypertrophy by targeting c-Jun. Nat Med. 2012;18:1643–50.
49. Sundaresan NR, Gupta M, Kim G, Rajamohan SB, Isbatan A, Gupta MP. Sirt3 blocks the cardiac hypertrophic response by augmenting Foxo3a-dependent antioxidant defense mechanisms in mice. J Clin Invest. 2009;119:2758–71.
50. Pillai VB, Samant S, Sundaresan NR, Raghuraman H, Kim G, Bonner MY, et al. Honokiol blocks and reverses cardiac hypertrophy in mice by activating mitochondrial Sirt3. Nat Commun. 2015;6:6656.